ผลของชนิดธาตุตัวที่สองในปริมาณน้อยที่มีต่อสมบัติของเซอร์โคเนียมไดออกไซด์

นางสาวจันทนา วิวัฒนพงศ์พันธ์

วิทยานิพนธ์นี้เป็นส่วนหนึ่งของการศึกษาตามหลักสูตรปริญญาวิศวกรรมศาสตรมหาบัณฑิต

สาขาวิชาวิศวกรรมเคมี ภาควิชาวิศวกรรมเคมี

คณะวิศวกรรมศาสตร์ จุฬาลงกรณ์มหาวิทยาลัย

ปีการศึกษา 2547

ISBN 974-17-7064-2

EFFECTS OF TYPES OF SECOND ELEMENTS IN SMALL QUANTITY ON ZIRCONIUM DIOXIDE PROPERTIES

Miss Jantana Wiwattanapongpan

A Thesis Submitted in Partial Fulfillment of the Requirements
for the Degree of Master of Engineering in Chemical Engineering
Department of Chemical Engineering
Faculty of Engineering
Chulalongkorn University
Academic Year 2004

ISBN 974-17-7064-2

Thesis Title	EFFECTS OF TYPES OF SECOND ELEMENTS IN SMALL QUANTITY ON ZIRCONIUM DIOXIDE PROPERTIES
By	Miss Jantana Wiwattanapongpan
Field of Study	Chemical Engineering
Thesis Advisor	Professor Piyasan Praserthdam, Dr.Ing.

Accepted by the Faculty of Engineering, Chulalongkorn University in Partial Fulfillment of the Requirements for the Master's Degree

…… Dean of the Faculty of Engineering
(Professor Direk Lavansiri, Ph.D.)

THESIS COMMITTEE

…… Chairman
(Montree Wongsri, D.Sc.)

…… Thesis Advisor
(Professor Piyasan Praserthdam, Dr.Ing.)

…… Member
(Waraporn Tanakulrungsank, D.Eng.)

…… Member
(Akawat Sirisuk, Ph.D.)

จันทนา วิวัฒนพงศ์พันธ์: ผลของชนิดธาตุตัวที่สองในปริมาณน้อยที่มีต่อสมบัติของเซอร์โคเนียมไดออกไซด์ (EFFECTS OF TYPES OF SECOND ELEMENTS IN SMALL QUANTITY ON ZIRCONIUM DIOXIDE PROPERTIES) อ.ที่ปรึกษา: ศ.ดร.ปิยะสาร ประเสริฐธรรม, 80 หน้า. ISBN 974-17-7064-2

การศึกษาผลของชนิดธาตุตัวที่สองที่เติมในเซอร์โคเนียมไดออกไซด์ที่สังเคราะห์ด้วยวิธีไกลโคเทอร์มอล โดยพบว่าการเติมธาตุตัวที่สองที่มีไอออนขนาดเล็กกว่าไอออนของเซอร์โคเนียมทำให้เกิดหมู่ไฮดรอกซิลขึ้น รูปร่างของเซอร์โคเนียมไดออกไซด์ที่ได้มีลักษณะกลมและการเติมธาตุตัวที่สองลงในเซอร์โคเนียมไดออกไซด์ทำให้อนุภาคที่ได้มีขนาดเล็กกว่าเซอร์โคเนียมไดออกไซด์ที่ไม่มีการเติมธาตุตัวที่สอง ขนาดผลึกของเซอร์โคเนียมไดออกไซด์ไม่มีความแตกต่างกันมากนักและมีค่าประมาณ 3 นาโนเมตร พื้นที่ผิวของเซอร์โคเนียมไดออกไซด์มีค่าสูง และการเติมธาตุตัวที่สองที่มีไอออนขนาดเล็กยังคงไว้ซึ่งพื้นที่ผิว ในขณะที่การเติมธาตุตัวที่สองที่มีขนาดไอออนใหญ่ทำให้พื้นที่ผิวลดลงอย่างมาก การเติมธาตุตัวที่สองที่มีไอออนขนาดเล็กทำให้เกิดการปรับปรุงเพิ่มตำแหน่งที่มีความเป็นเบสและหมู่ไฮดรอกซิลขึ้น ส่งผลให้มีการดูดซับก๊าซคาร์บอนไดออกไซด์เพิ่มมากขึ้น แต่ให้ผลตรงข้ามสำหรับการเติมด้วยธาตุที่มีไอออนขนาดใหญ่ การเติมธาตุที่มีไอออนขนาดเล็กลดปริมาณของ Zr^{3+} อย่างมากแต่การเติมไอออนที่มีขนาดใหญ่ เช่น ตะกั่วและบิสมัท ทำให้ปริมาณของ Zr^{3+} เพิ่มขึ้นอย่างมาก

ภาควิชา……..วิศวกรรมเคมี……. ลายมือชื่อนิสิต……

สาขาวิชา…….วิศวกรรมเคมี…… ลายมือชื่ออาจารย์ที่ปรึกษา……

ปีการศึกษา…..2547……

4670255921: MAJOR CHEMICAL ENGINEERING
KEY WORD: ZIRCONIA / THE SECOND ELEMENT / GLYCOTHERMAL METHOD

JANTANA WIWATTANAPONGPAN: EFFECTS OF TYPES OF SECOND ELEMENTS IN SMALL QUANTITY ON ZIRCONIUM DIOXIDE PROPERTIES. THESIS ADVISOR: PROFESSOR PIYASAN PRASERTHDAM, Dr.Ing. 80 pp. ISBN 974-17-7064-2

To study the effect of types of the second elements added in zirconia synthesized by glycothermal method. It was found that occurrence of hydroxyl group depended on cationic size, positive result when small ionic size added. The morphologies of all products observed by SEM were spherical and secondary particle seems smaller than undoped zirconia. The crystallite size of all samples was not different and in values about 3 nm. High surface area was maintained when doping with small cationic size and the result in contrast when large cationic size added. The basic property and hydroxyl groups of zirconia were improved consequently to much adsorption of CO_2 when the second element added in appropriate quantity but this depended on cationic size, big ionic size give negative effect. The Zr^{3+} quantity was increased markedly when big ionic size such as lead and bismuth added.

Department ... Chemical Engineering… Student's signature……..
Field of study...Chemical Engineering… Advisor's signature……..
Academic year…….2004……

ACKNOWLEDGEMENTS

The author would like to express his greatest gratitude to her advisor, Professor Dr. Piyasan Praserthdam, for his invaluable suggestion and guidance throughout this study. In addition, I would also grateful to thank to Dr. Montree Wongsri who has been the chairman of the committee for this thesis, Dr. Waraporn Tanakulrungsank and Dr. Akawat Sirisuk, members of the thesis committee for their kind cooperation.

Best regards are expressed to Miss Patta Soisuwan, Dr. Okorn Mekasuvandamrong and many friends in Center of Excellence on Catalysis and Catalytic Reaction Engineering who always provide the encouragement and co-operate along the thesis study.

Moreover, the author would like to thank the Thailand Research Fund (TRF), the Thailand-Japan Technology Transfer Project (TJTTP) as well as the Graduate School of Chulalongkorn University and Center of Excellence on Catalysis and Catalytic Reaction Engineering for their financial support. Finally, she also would like to dedicate this thesis to her parents for their worthy support and encouragement at all times.

CONTENTS

Page

Page

LIST OF TABLES

LIST OF FIGURES

Figure Page

Figure Page

CHAPTER I

INTRODUCTION

Nowadays, zirconium dioxide (ZrO_2) or zirconia is an important material and has obtained much interest in industry. In zirconia composites, the martensitic transformation from tetragonal to monoclinic zirconia produces materials with high toughness. When zirconia is doped with divalent or trivalent cations, its structure is deficient in oxygen, which favors oxygen transportation and produces ionic conduction. Therefore, zirconia can be used as an oxygen sensor and in the fabrication of fuel cells. It has high thermal and chemical stability, high strength, corrosion resistance, unique double function character of weak acidic and basic properties as well as low conductivity. Those are useful in many fields such as ceramics, electronics including catalysis such as catalysts and catalyst supports.

As electrolyte for SOFC, doped zirconia with a lower valence cation has been regarded as the most promising material with high ionic conductivity and transference number of oxide ions which is operative at high temperatures around 1000 ^{o}C (Eguchi *et al*., 2000 and Lee *et al*., 2001).

As a catalyst showed promising results in environmental catalysis, such as threeway catalyst for automotive exhaust (Loong and Ozawa, 2000), photocatalytic reaction (Silvia *et al*., 1999), dehydration of alcohol (Das *et al*., 2002), CO hydrogenation (Caili *et al*., 2000), hydrolysis (Yinghong *et al*., 2003).

Reactions of zirconia catalyst support are CO oxidation and NO reduction (Wei *et al*., 1996), *n*-butane isomerization (Carlos *et al*., 2002 and Yongde *et al*., 1999), hydrogenation, methanol synthesis, Fischer-Tropsch reaction (Zhou *et al*., 2003).

Therefore, to study factor affected on properties of zirconia are important and interested. The main purpose of this research is to investigate effects of the second

elements added in glycothermal zirconia on the properties for example; chemical and physical properties. Carbon dioxide adsorption was used to characterize the surface properties, which are used to identify an amount of basic site on surface by many authors. The scopes of this study are as the following

1. Zirconium dioxide powders are synthesized via glycothermal method. Both reaction temperature and amount of second elements at various ratios are fixed to determine the appropriate quantity of each second element. Values of second element content and reaction temperature investigated are in the range of 0.002-0.005 molar ratio and 300^{o}C, respectively.

2. Types of second elements selected were considered to vary ion charge +3 for Al, Ga and Bi, charge +4 for Si and Pb and for charge +5 for P, and the same group was considered to vary ion size in shell K-L-M for Al^{3+} (0.54 Å), Si^{4+} (0.4 Å), P^{5+} (0.38 Å), in shell L-M-N for Ga^{3+} (0.62 Å), in shell N-O-P for Pb^{4+} (0.94 Å) and Bi^{3+} (0.1.17 Å).

3. Effects of types of second elements on properties of zirconium dioxide products are characterized as the following:

- Surface area is measured by BET method.
- Crystallite size and phase identification are performed by X-ray diffraction.
- Amount of CO_2-adsorbed is determined by temperature programmed desorption (CO_2-TPD).
- Morphology is illustrated by using a scanning electron microscope (SEM).
- Functional group over zirconia surface is evaluated by infrared spectroscopy (IR).
- Amount of Zr^{3+} intensity is measured by electron spin resonance (ESR).

The present study is arranged as follows:

Chapter II presents literature reviews of the previous works related to this research.

Chapter III explains the basic theory about zirconia such as the general properties of zirconia and the various preparation methods to obtain the ultrafine zirconia.

Chapter IV shows the experimental equipment and systems, and the preparation method of zirconia by the glycothermal method.

Chapter V exhibits the experimental results.

In the last chapter, the overall conclusions of this research are given.

Finally, examples for calculation of the required amount of the starting materials and crystallite size are included in appendices at the end of this thesis.

CHAPTER II

LITERATURE REVIEWS

There have been several studies on the role of dopant on the physical properties of zirconia. An effect of additive ionic radius on lattice parameters of zirconia has been studied extensively by many researchers. Wen *et al*. (1997) studied crystal structure of zirconia by doping rare earth oxide and showed the differential of lattice parameters increased with dopant radius. These results are consistent with a work of Elisabeth *et al.* (2003). They investigated an influence of the substitution of Zr^{4+} by oversized rare earth R^{3+} (Sc, Yb, Y, Gd, Sm). It is concluded that an extension of c lattice parameter is strongly dependent on the cationic size dopant. This indicates that zirconia and cation form a complete solid solution (Khor *et al*., 1997). Large tensile stresses were observed for oversized dopant when increasing the amount of doping element alike increasing the ionic radius of dopant. Hunter *et al.* (1999) investigated factors influencing the stability of the tetragonal phase. The stability has been said to be influenced by tetragonality (*c/a* ratio), the number and distribution of oxygen vacancies associated with the size of the dopant ions. It was found that when substituted tetravalent ions (Ge, Ti, Sn and Ce) into tetragonal zirconia, a mean value of cation-anion bond length varied linearly with the concentration of the substituent ions, where the bond length increased or decreased depending on whether the substituted ion is larger or smaller than the zirconium ion it replaces. Therefore, size, valence and location of incorporated ion might be the decisive parameters to change unit cell volume (Friderike *et al*., 2004). Changing of cell volume occurred when Zr cations were replaced by smaller size of Sn ions; however aspects of unit cell were changed randomly and did not depend upon ionic radius of dopant corresponded to a result of Jang *et al*. (2004). In addition, Vladimir *et al.* (2003) found that unit cell volume decreased with increasing smaller aluminum ion content.

The lower valence (Al^{3+}) (Friederike *et al*., 2004 and Vladimir *et al*., 2003) and oversized dopant (Y^{3+}) (Wei *et al*., 1996) introduced oxygen vacancies located as nearest neighbors to Zr^{4+} ions to compensate charge balance, then undersized

tetravalent dopant (Ti^{4+}) competes with Zr^{4+} ions to form oxygen vacancies in zirconia, which were almost occurred nearby Ti^{4+}. On that basis, it is believed that there are two kinds of oxygen vacancy associated with cations as following; Zr-V_O-Zr and Ti-V_O-Ti in the zirconia lattice (Capel *et al*., 1999). These vacancies increase the electrical conductivity with diffusing oxygen ions being the primary charge carrier.

Many studies have demonstrated that the oxygen vacancies of metal oxides can enchance the activities of these catalysts for CO oxidation and CO hydrogenation (Wei *et al*., 1996) because of the higher oxygen mobility (Dongare *et al*., 2001). The addition of Al or Cs into ZrO_2 could largely enhance the activity (Yingwei *et al*., 2004b) and adding the small amount of Cr, Mn and Ca into ZrO_2 made rising of reaction rate for hydrogenation of aromatic acids reaction (Iglesia *et al*., 1997). In addition, Carlos *et al*. (2002) found that catalytic activity for isomerization reaction is supposedly related to charge abstraction from radical and ionic intermediates, a process enabled or enhanced by ionic vacancies in tetragonal zirconia catalysts. Yue *et al.* (2003) prepared ZrO_2 by precipitation and impregnation in range of 2-10 wt% potassium to use as catalysts for CS_2 hydrolysis. The hydrolysis over ZrO_2 is only slightly increased after adding potassium, and it decreases significantly at high loading. For zirconia catalyst with greater amount of surface basic sites, the role of akali dopant is positively presented at low loading, and a negative effect is observed at high loading due to the loss of specific surface area after doping.

Caili *et al*. (2000) study acidic and basic properties of zirconia by CO_2-TPD and NH_3-TPD for isobutene synthesis. They suggested that basic sites are responsible for the chain propagation to form i-C_4H_8 and would be necessary catalytic sites to remove active hydrocarbon from the intermediates of the reaction. Acid sites are responsible for the activation of reactant molecule. This supported with Kenichi *et al*. (2000) and Yingwei *et al*. (2002). They found that basicity is available for the aldol condensation reaction to form C_3 hydrocarbons from the C_2 oxygenate and branched C_4 compounds from C_3 oxygenate.

Yoshida *et al*. (2003) study active sites on silica-supported zirconium oxide for photoinduced direct methane conversion and photoluminescence. They reported that Zr-O-Si linkage would be the photoactive site. But forming of linkage will be occurring then one type metal loading would be small amount to highly disperse, otherwise phase oxide separated will be happened. Kongwudthiti *el al*. (2003b) studied SiO_2-modified ZrO_2 with various Si/Zr ratios prepared by glycothermal method. They found that the presence of Si-O-Zr bonds retards the crystal growth upon calcination and can stabilize tetragonal phase.

The role of dopant on phase stabilization was reported that when amount of dopant oxide is increased, the monoclinic peak intensity gradually decreases and disappears (Boulouz *et al*., 1999). Due to the incorporation of dopant into a ZrO_2 matrix leads to a transformation of phase from monoclinic to tetragonal with a distortion of the lattice (Silvia *et al*., 1999) Valmalette *et al*. (2002) found that decreasing particle size stabilized tetragonal zirconia to reduce surface energy. While Bokhimi *et al*. (1998) reported OH^- ions and Zr vacancies in crystalline structure stabilized the tetragonal phase. Both defects disappeared when samples were annealed at high temperatures, which brought about the irreversible transformation of the tetragonal into the monoclinic structure. Moreover, anionic vacancies in zirconia were proposed to be stabilizer for tetragonal phase (Carlos *et al*., 2002). Francisco *et al*. (2000) studied SiO_2-ZrO_2 mixed oxide, they attributed the presence of Si-O-Zr at low Si loading as chemical impurity which responsible for tetragonal zirconia stabilization.

There have been several studies on surface defect of zirconia. Takeuchi *et al.* (1995) studied the influence of surface defects of by using Argon ion sputtering to increase the surface defects. It is found that many surface defects were produced. When water is adsorbed on the ZrO_2 surface, it dissociates producing hydrogen and supplying oxygen atoms to the lattice of defects. While Rose *et al.* (1997) investigated the correlation of defect density to the grain size in Pd and ZrO_2, synthesized by the inert gas condensation technique with different initial grain sizes and were irradiated using 4 MeV Kr ions. It was found that defect density rapidly decreased when grain

size below 50 nm. In the smallest ZrO_2 and Pd grains below 15 and 30 nm respectively, could not be detected defects. In addition, surface properties of ZrO_2 were studied by ESR method. Qin *et al.* (2004) studied intensity of Zr^{3+} when zirconia was placed in different atmospheric conditions, i.e., He, H_2, O_2, air and wet air at temperatures ranging from 25-600 ^oC. The Zr^{3+} centers can be described as the oxygen coordinatively unsaturated Zr sites. More Zr^{3+} centers were formed on the surface of ZrO_2 by treating the sample in He at temperatures above 400 ^oC and the formation of the Zr^{3+} centers may be associated with the removal of surface hydroxyl. Zr^{4+} in ZrO_2 cannot be reduced at temperatures of up to 600 ^oC in H_2, while some surface hydroxyl can be reduced by H_2 to form F-center at temperatures higher than 250 ^oC. In H_2 at temperatures above 400 ^oC, O_2^- can be formed from the Zr^{3+} centers and F-centers, and its formation may be concerned with both H_2 and the trace amount of O_2 in H_2. Whereas in O_2, amount of Zr^{3+} as a function of partial pressure of O_2 which coordinatively unsaturated occurred on surface of ZrO_2 can be active sites in some reaction because of strong interaction with reactant gas such as H_2, CO and alkene.

Effect of the dopant content on the optical property of Y_2O_3, CaO doped zirconia was investigated by Boulouz *et al*. (1999). They reported that the refractive index of the cubic zirconia decreases as the mole percent of Y_2O_3 or CaO content is increased. This functional dependence would be expected since as the Y_2O_3 (or CaO) concentration is increased there is an increase in vacancies generated because of the different valence state of Zr^{4+}, Y^{3+} and Ca^{2+}. While Hartridge et al. (2001) claimed that decreasing in refractive index with increasing in ionic size can be attributed to the increase in lattice parameter with ionic size of dopant and also correlated with the decrease in electrical conductivity.

Lee *et al*. (2001) studied the electrical property of yttria-doped ceria-stabilized zirconia. It was found that the electrical conductivity and the electrolytic domain boundary of CeO_2-ZrO_2 are greatly enhanced by yttria doping. The electrical conductivity increased as the doping level increased. However, the degree of enhancement is gradually decreased as the doping level increased up to 15 m/o, then it decreased rapidly. They mentioned that this phenomenon resulted from the clustering

of the defects or vacancy ordering due to the increase of defect concentration. When the size difference between constituent ions could be created oxygen vacancies. In Ce-doped ZrO_2 system, Cerium ion is much larger than zirconium ion, this size difference could encourage the additional defect creation and is called size effect. On the other hand, in yttria-doped CeO_2-ZrO_2 system, Y^{3+} has a lower valent cation occupying a Zr^{4+} or Ce^{4+} creates oxygen vacancies, which induce the enhancement of ionic conductivity and electrolytic stability at small doping but results is opposite at higher doping concentration. It reduces defect association.

Many researchers investigated effect of dopant on surface. Silvia *et al*. (1999) studied increasing surface area with the Fe content in zirconia. While Zhao *et al*. (2004) and Kongwudthiti *et al*. (2002) reported that Si doping could increase the surface area, retard the grain growth, stabilize the tetragonal phase of zirconia powders and preserve the tetragonal phase even after calcination at high temperature.

From the list of literatures, the objective of this study is, hence, to study the effect of types of second elements on zirconia properties under glycothermal condition.

CHAPTER III

THEORY

3.1 Chemical properties

Zirconium tetra *n*-propoxide $Zr(OC_3H_7)_4$, molecular weight of 327.6, is a yellow-brown liquid; density, d = 1.05 g/ml; solidification point below -70^oC; flammable, flash point below 21^oC; soluble in hydrocarbons. Usually, zirconium alkoxides hydrolyze in moist air.

Table 3.1 Ionic radius of dopant elements (Aylward and Findlay, 2002).

Element	Ion charge	Ionic radius (Å)		
		Coordination number		
		4	6	8
Zr	4+	0.59	0.72	0.84
Si	4+	0.26	0.4	
Al	3+	0.39	0.535	
P	3+		0.44	
	5+	0.17	0.38	
Ga	2+		1.2	
	3+	0.47	0.62	
Pb	2+	0.98	1.19	1.29
	4+		0.78	0.94
Bi	3+		1.03	1.11
	5+		0.76	

3.2 General feature of zirconia

Zirconia has three polymorphs, the monoclinic (space group *Fm3m*), tetragonal (*$P4_2/nmc$)*, and cubic phases (*$P2_1/c$*). Crystal structures of cubic, tetragonal and monoclinic zirconia are shown in Figure 3.1. Tetragonal and cubic are metastable

whereas monoclinic are thermodynamically phase. The monoclinic is stable up to about 1200^{o}C (Yingwei *et al*., 2004a), at which temperature it transforms into the tetragonal phase (Garvie, 1978), which is stable up to 2370^{o}C. Above 2370^{o}C, the cubic phase is stable and it exists up to the melting point of 2680^{o}C (Bikramjit *et al*., 2004).

Zirconium dioxide is normally monoclinic at room temperature but tetragonal phase can exist at room temperature (Garvie, 1997). The stabilization of tetragonal zirconia is important in use of zirconia for phase purpose. Zirconia preparation methods are precipitation from alkaline aqueous solution, by calcination of zirconyl nitrate at low temperature, by the presence of small amount of impurity (Bikramjit *et al*., 2004), by glycothermal method (Kongwudthiti *et al*., 2003a). The tetragonal appeared was attributed to size effect. Many researchers reported that tetragonal appeared to be a critical crystallite size about 30 nm and above that tetragonal could not stabilized at room temperature. They described about lower surface energy in the tetragonal phase (0.77 J/m^2) compared to the monoclinic phase (1.13 J/m^2) (Garvie, 1965). The transformation of the metastable tetragonal form into the monoclinic form is generally complete by 650-700 ^{o}C.

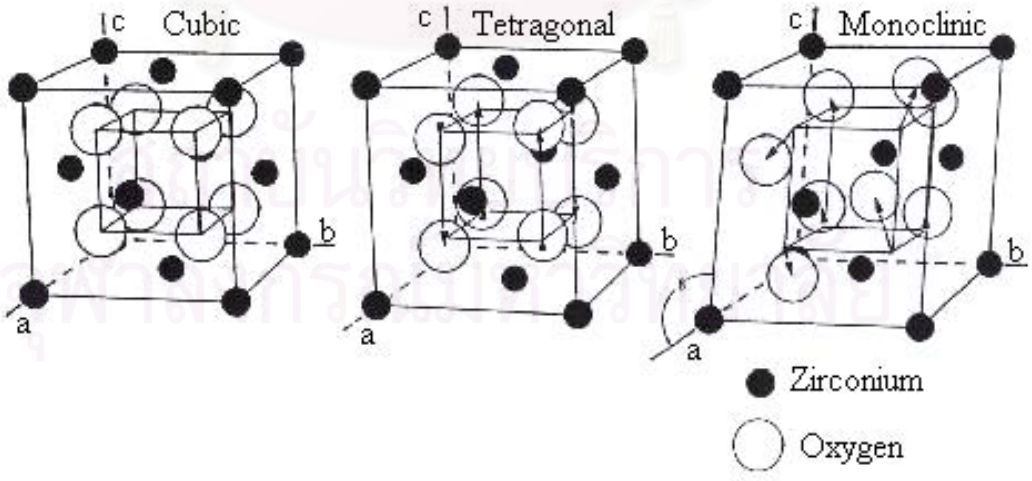

Figure 3.1 Crystal structures of cubic, tetragonal and monoclinic zirconia.

3.3 Preparation of zirconia by glycothermal method

The synthesis method for producing zirconia has many methods, which are under intensive worldwide investigation for powder preparation. In this part, the use method in this thesis is described below.

Glycothermal method has been developed from hydrothermal method for synthesis of metal oxide and binary metal oxide, by using glycol as the reaction medium under pressure and at temperatures above its normal boiling point. The use of glycol instead of water in the hydrothermal method produced the different form of intermediate phase and the stability of such intermediate phase was not strong. The preparation method is described in the experimental section, Chapter IV.

3.4 Type of defects

Defects can be broadly divided into two groups: stoichiometric defects in which the crystal composition is unchanged on introducing the defects and non-stoichiometric defects, which are a consequence of a change in crystal composition. Some phenomena cannot be explained without leading the presence of defects. These include:

1. Understanding the forces required fracturing a crystal. If one simply calculated the force required to separate two layers of atoms in a crystal, the result would come out to be much larger that the actual force required fracturing a solid. It therefore appears as if a crystal breaks in stages, with each stage requiring a rather smaller force.

2. The ability of a crystal to deform irreversibly under stress. The primary example is called slip. Where application of a stress acts as a shear stress on particular crystal planes that appear to slide over each other.

3. The origin of color in many materials that would otherwise be transparent. A well-known example is the red color of ruby, Al_2O_3, which is caused by Cr^{3+} impurities on the Al sites

4. The presence of a small but non-zero electrical conductivity in insulators, these are caused by the motion of charged ions as in a salt solution. Ionic conductivity is much higher in materials that contain vacant sites as defects.

5. The ability of atoms to diffuse within a solid, such as the diffusion of carbon atoms in iron. The processes are related to those that allow electrical conductivity.

6. Crystal growth, which often appears to proceed through a process that, involves the formation of a spiral defect.

The presence of defects can be exploited in applications, and in other cases the presence of defects causes technological problems, and both mean that it is important to understand the behavior of defects. Two such defects particular importance is the Frenkel and Schottky defects. Only point defect that concerns our work thus large-scale imperfections will not mentioned in details. The details of point defects are following

3.4.1 Vacancies: Schottky defects

Consider the simplest crystal defect, namely that of an atomic site becoming vacant, with the missing atom migrating to the crystal surface. This process will be energetically unfavorable, costing the system a change in energy.

The simple case of a vacant site is called a Schottky defect. In order to maintain a neutral charge distribution across a local length scale, it is common for both positive and negative vacant sites to be produced in thermal equilibrium and to be evenly distributed throughout the sample. This is represented in Figure 3.2.

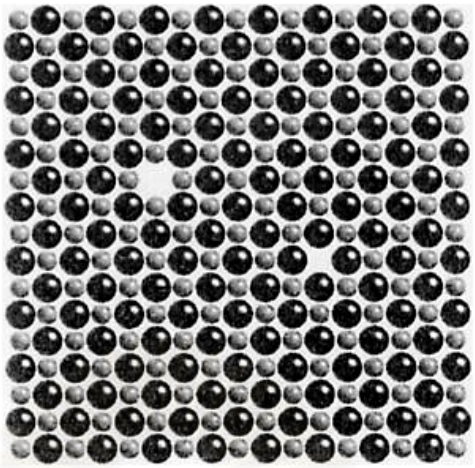

Figure 3.2 Cation and anion charge-balanced Shottky defects in NaCl.

3.4.2 Interstitial defects: Frenkel defects

In crystals that not pack with high efficiency, it is possible for atoms to occupy sites that are normally vacant, called interstitial sites. A Frenkel defect occurs when at atom leaves its normal site to create a vacancy, and is then displaced into one of the interstitial sites. This process is illustrated in Figure 3.3.

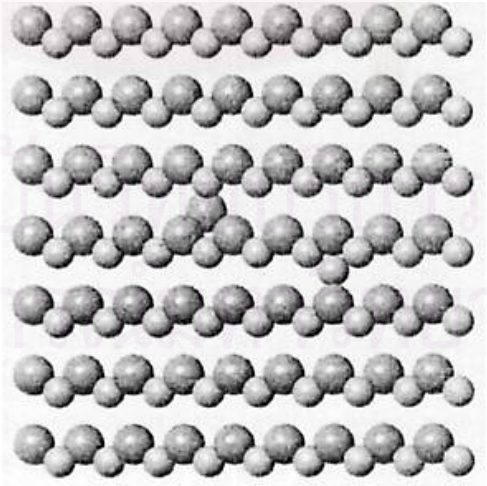

Figure 3.3 Pair of charge-balanced Frenkel defects in AgI.

3.4.3 Coupled charge substitutions and vacancies

The vacancies that mentioned above occur as equilibrium processes. Other point defects can be produced as non-equilibrium structures through the process of crystal growth. A common defect is the substitution of a different type of atom, usually one of similar charge. For example, NaCl can contain K^+ defects substituting for the cation sites, or F^- substituting on the anion sites. A substitution of a different charged cation will require production of a compensating charge defect. For example, substituting a Ca^{2+} cation in NaCl will require the formation of a charge-compensating cation vacancy. This structure is illustrated in Figure 3.4.

Figure 3.4 Substitution of a Ca^{2+} cation for a Na^+ cation in NaCl, accompanied by the formation of a vacant cation site in order to maintain charge neutrality.

3.4.4 Color centers

The charge substitutions that have considered have been restricted to ions. It is also possible for electrons to occupy vacant anion sites in order to maintain charge neutrality. The electron forms its own energy bands. The color center is able to absorb electromagnetic radiation in the visible spectrum, and this gives color to what would otherwise be a transparent crystal. As a result, the presence of the color center can be detected in an optical absorption experiment.

3.5 Surface defects

There is a sense in which the surface itself with its coordinatively atoms it the most numerous type of defect. The bulk of the experimental results, spectroscopic or otherwise, necessarily relate to adsorption on the more numerous and expected sites on oxide surface, such as coordinatively unsaturated cations or anions, hydroxyls, acid-base pair, etc. However the most active sites will be connected with defects in the normal surface, which have unusual geometrical and/or local chemical compositional features. These may be present in concentrations that are one or two orders of magnitude less than those of the regular sites and their experimental detection can be correspondingly different.

In general, the majority of the experimental phenomena discussed above were connected with adsorption on the more numerous and expected sites on the oxide surface (coordinatively unsaturated cations, anions, hydroxyls, and their pair). However, the appearance of the most active surface centers suggests a connection with defects in the solid. The other factors influencing the properties of the real oxide surfaces are: (i) the presence of different lattice defects in the surface layer, and (ii) their chemical composition, which in many cases, may differ from that in the bulk.

In spite of the fact that the concentration of the defect centers on the surface is one or even two orders of magnitude less than the concentration of regular active sites, their reactivities are very often higher. This is why such defect centers can participate in the reaction.

The presence of the so-called dangling bonds (unsaturated valencies) at the surface creates electron energy states, usually named intrinsic states, which are present even in the case of pure and strictly stoichiometric surface. Additional structural defects on the surface which may be or may be not associated with adsorbed impurities, said to create extrinsic surface states.

The role of intrinsic defects in the activation of adsorbed molecules has not yet been elucidated. The physics of such defects is also still in development. In contrast,

the influence of extrinsic defects on chemisorption and catalysis has been the object of many investigations.

Crystal with periodical arrangements of all of their structural elements cannot exist and real crystals show the presence of various imperfections described as defects. Those atoms into other sites or interstitial positions may due to (i) the displacement of atoms from the lattice sites normally occupy them, (ii) the presence of some vacant sites, or (iii) the displacement of part of a crystal with respect to another part along a crystal plane, etc. These defects are usually classified according to their dimensions into point defects (vacancies interstitial or foreign atoms), linear defects (dislocations) and spatial defects such as pores of foreign inclusion. For example, besides being a strong base, the highly dehydroxylated MgO surface is a good reducing agent. The reducing sites are apparently defects, possibly surface cation vacancies: the dissociative chemisorption of Bronsted acids blocks the reactivity of the reducing sites.

Investigation of small-surface-area bulk alkali earth-metal oxides, including MgO, e.g. as single crystal, show that their photoluminescence is caused by defects in the crystalline lattice, namely by the F^+ and $F^\bullet$ centers, i.e. the oxygen vacancies have captured one or two electrons, respectively. Such centers can be easily detected directly by EPR and/or by UV-Vis spectroscopic studies of the adsorption of molecules that easily form cation or anion radicals. Detailed analysis of such spectra obtained by using molecules which different but known values of ionization potential (IP) or electron affinity, allows us to obtain information about such an adsorption center, for example, on the basis of data on the transition to the radical state, and so to make a conclusion about its redox properties.

The main method used to investigate such centers is electron paramagnetic resonance (EPR) spectroscopy. It should be remembered that the formation of radicals could proceed on the surface of practically all oxide systems, when easily ionizable adsorbates which are able to cause the formation of both main and side-reaction products, are used.

In connection with the problem of defect sites, studies of mechanically activated oxide systems seem to be very interesting and useful. It is well known that mechanical activation (by grinding) affects an increase in the number of defects formed upon mechanical activation.

Mechanical treatment is an effective method for creating defects in solids. Various mechanical activation effects are related to the formation of such defects and their subsequent chemical transformations. Some of these defects are free radicals, for example in the case of SiO_2 $(=Si\text{-}O\text{-})_3Si^{\bullet}$ and $(=Si\text{-}O\text{-})_3SiO^{\bullet}$. A new type of natural defect, namely silanone (Si=O) groups was identified on the surface of mechanically activated SiO_2. A study was carried out by using their thermal stabilities, optical properties (a characteristic absorption band was found with a maximum at 5.3 eV) and reactivities, relative to simple molecules, such as CO_2 and N_2O, and radicals, such as H, D and CH_3. Studies of the IR and Raman spectra of the oxides MgO, Cr_2O_3, MoO_3, Co_3O_4 and CuO in the regions of the cutoff vibrations allowed identification of sample amorphization during mechanical activation and also the decrease in the coordination number of both cations and anions as compared with nonactivated oxides. The latter bring to increases in the reactivities. According to IR spectra of adsorbed CO in the case of CuO and Co_3O_4, the reduction of Cu^{2+} to Cu^{+} and Co^{3+} to Co^{2+} cations was observed during mechanical activation.

In the diffuse reflectance electron spectroscopy (DRES) spectra of MoO_3, the valence-to-conduction band transition exhibited a considerable blue shift with decreasing particle size. Excitonic absorptions observed in these spectra are also affected by the smaller particle size and by the altered crystallite surface. An increasing intensity of the bands was observed, and a linear dependence between the position of the band attributed to polaron conductance and the logarithm of the carrier concentration per Mo atom was obtained, both of these fact reveals that a sub-stoichimetric MoO_{3-x} species was formed upon mechanical treatment. According to the ESR data, both milled and non-milled MoO_3 samples contained Mo^{5+} centers interacting with OH groups in close vicinity, but their concentration was much smaller in the case of non-milled MoO_3. The main portion of these Mo^{5+} ions had C_{2v} or C_{4v} symmetry. These latter ions appear to result from the mechanical activation

process and are suggested to be the precursors of a crystallographic shear structure. Exposure to O_2 reveals that all of these Mo^{5+} sites are located in the bulk and not necessarily on the surface, whereas free electrons are present at the surface. The high surface sensitivity of the IR technique when using adsorbed probe molecules revealed the formation of coordinatively unsaturated Mo^{4+} surface states in MoO_3 which was mechanically activated.

3.6 Surface hydroxyl groups

Actually, the broken bonds on the crystal surface become saturate as a result of dissociation of the H_2O molecules: hydrogen is bonded to an oxygen atom, whereas the hydroxyl groups bond the metals atoms. The appearance in the spectra of several bands characteristic of hydroxyl groups, as well as their different spectral characteristics and chemical properties (acidity, reactivity), are due to the exposure of several crystal faces and different kind of defects on the oxide surface. Practically every study of surface properties and/or adsorption of molecules on oxides provides data about surface hydroxyl groups.

After oxide dehydration at high temperature and following the removing of bound molecular water, the bands caused by OH vibrations (which can be regarded as localized vibrations of the adsorbed atom (H) on the surface) are observed at frequencies higher than those of the lattice cutoff absorption. For most oxides, the vibrations of bonds of isolated hydroxyl groups appear in the IR spectra as discrete absorption.

Oxides that had been heated at only moderate temperatures exhibit several other bands, the appearance of which depends on the preparative conditions and pre-treatment temperature. In general, the IR band due to the OH stretching vibration of a hydroxyl group appears at a lower wave number, is strengthened in integrated intensity and is broadened, if the group is involved in hydrogen-bonding interaction.

It is now clear that the spectral features of isolated surface hydroxyl groups depend on the chemical structures of the oxides, and their detailed interpretation

conversely enables conclusions to be drawn about the structures of the oxide surfaces and about their active sites.

A reason for the appearance of several bands due to free surface hydroxyl groups in the IR spectra is the capability of the oxygen atoms of the OH groups to be in contact with several immediate neighboring metal atoms. Hence, the number of the latter should exert a decisive influence on the vibrational frequency, νOH, which is observed. For isolated (free hydroxyl groups, the oxygen can be bound to one, two, three, etc., metal atoms (types I, II, III, etc).

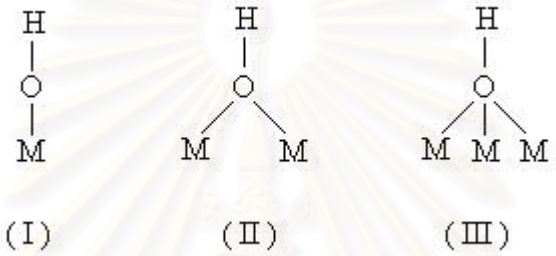

The oxygen of the OH group can form bonds with several metal atoms if this allowed by their mutual arrangements. The oxygen atoms of the surface OH groups always occupy those positions where the O atoms would have been present in the infinite lattice. The number of metal atoms around the oxygen of an OH group is always smaller than the coordination number in the lattice, i.e. the maximum number of OH groups for the oxide in question equals the oxygen coordination number minus one.

3.7 CO_2 Temperature programmed desorption (CO_2-TPD)

This technique is the principle of CO_2 adsorption at surface. After saturation, the temperature was increased gradually and CO_2 was desorbed from surface and detected by TCD gas chromatography until constant signal. To measure basic site, which amount of CO_2 desorbed, will be indicate basicity. CO_2 chemically adsorption was occur on surface oxygen, hydroxyl group.

CHAPTER IV

EXPERIMENTAL

The experimental system and procedures in the synthesis of zirconia are presented in this chapter. The chemicals and experimental equipment are shown in sections 4.1 and 4.2, respectively. In section 4.3, the preparation and characterization of products are explained.

4.1 Chemicals

Zirconia powders were synthesized with the following reagents:

1. Zirconium tetra-*n*-propoxide (ZNP, $Zr(OC_3H_7)_4$)
2. Tetraethyl orthosiliocate (TEOS, $(C_2H_5O)_4Si$)
3. Aluminium isopropoxide (AIP, $Al(OC_3H_7)_3$)
4. Triethyl phosphate (TEPP, $P(O_4C_6H_{15})$)
5. Gallium (III) acetylacetonate ($Ga(C_5H_8O_2)$)
6. Lead (IV) acetate ($Pb(C_2H_3O_2)_4$)
7. Bismuth (III) acetate ($Bi(C_2H_3O_2)_3$)
8. 1,4 Butanediol ($HO(CH_2)_4OH$)

The calculation of the amount of reagents required in the reaction is shown in Appendix A.

4.2 Equipment

The equipment for the synthesis of zirconia consisted of:

4.2.1 Autoclave reactor

- Made from stainless steel
- Maximum temperature of 350^{o}C

- Pressure gauge
- Relief valve used to prevent runaway reaction
- Test tube was used to contain the reagent and glycol

Autoclave reactor used for the experiment is shown in Figure 4.1.

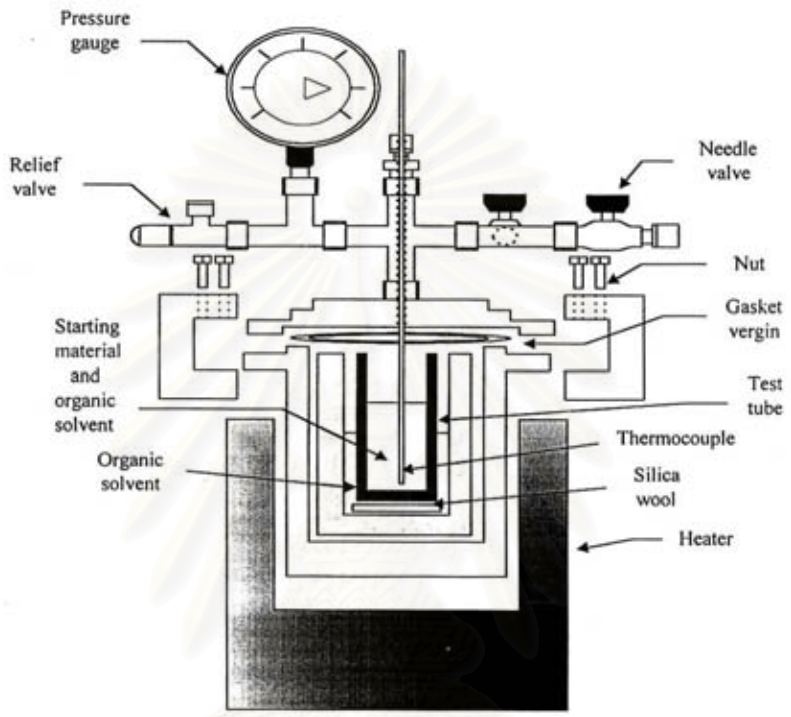

Figure 4.1 Autoclave reactor.

Experiments

- Autoclave volume of 1000 cm^3 and an iron jacket was used to reduce the volume of autoclave to be 300 cm^3.
- Thermocouple is attached to the reagent in the autoclave.
- Amount of starting material = 7 g
- Amount of organic solvent in the test tube = 100 cm^3
  and amount of organic solvent in the gap between test tube and autoclave wall = 30 cm^3

4.2.2 Temperature program controller

A temperature program controller was connected to a thermocouple attached to the autoclave.

4.2.3 Electrical furnace (Heater)

Electrical furnace supplied the required heat to the autoclave for the reaction.

4.2.4 Gas controlling system

Nitrogen was set with a pressure regulator (0-150 bar) and needle valves were used to release gas from autoclave.

The diagram of the reaction equipment for the synthesis of zirconia is shown in Figure 4.2

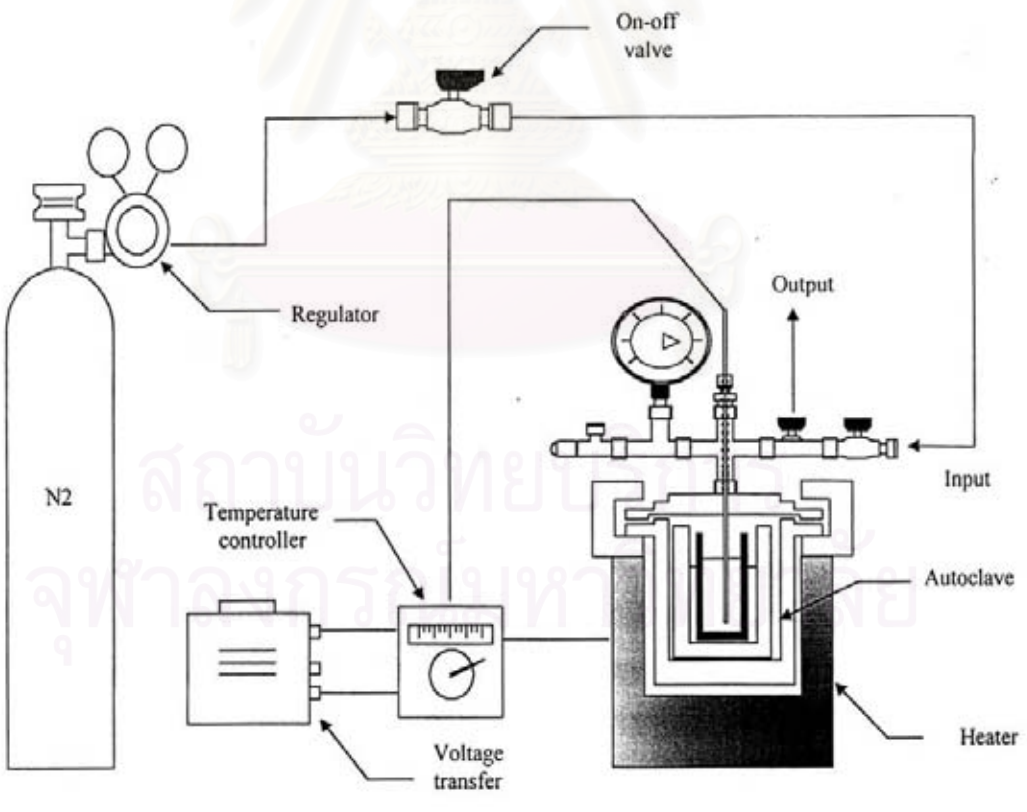

Figure 4.2 Diagram of the reaction equipment for the synthesis of zirconia.

4.3 Preparation of zirconia

4.3.1 Undoped zirconia

Zirconia was prepared by using zirconium *n*-propoxide 7 g as a starting material. The starting material were suspended in 100 ml of 1,4 Butanediol in the test tube, and then set up in the autoclave. In the gap between the test tube and autoclave wall, 30 ml of the glycol was added. After the autoclave was completely purged with nitrogen, the autoclave was heated to a desired temperature (200^oC-300^oC) at a rate of $2.5^oC\ min^{-1}$ and held at that temperature for 2 hours. Autogeneous pressure during the reaction gradually increased as the temperature was raised. After the reaction, the autoclave was cooled to room temperature. The resulting powders were collected after repeated washing with methanol by centrifugation. They were then air-dried.

4.3.2 Second elements doped zirconia

For the synthesis of zirconia doping with dopant, the method is the same as that for pure zirconia synthesis except the starting material, i.e. the mixture of zirconium *n*-propoxide 7 g and an amount of dopant such as Si, Al, P, Ga, Pb and Bi at metal/Zr ratio of 0.002-0.02 was used as the starting material (see Appendix A).

4.4 Catalyst Characterization

4.4.1 X-ray Diffraction Spectroscopy (XRD)

The X-ray powder diffraction (XRD) patterns were obtained on an X-ray diffractometer. The crystallite size was estimated from line broadening according to the Scherrer equation (see Appendix B) and α-Al_2O_3 was used as a standard.

Model of XRD for experiments: Siemens D5000 using nickel filtered CuKα radiation at Center of Excellences on Catalysis and Catalytic Reaction Engineering, Chulalongkorn University.

4.4.2 Scanning Electron Microscopy (SEM)

Morphology and size of secondary particle of the samples were observed by scanning electron microscope (SEM).

Model of SEM for experiments: JSM-5410LV at the Scientific and Technological Research Equipment Center, Chulalongkorn University (STREC).

4.4.3 Surface Area Measurement

The specific surface area of the samples was calculated using the Brunauer-Emmett-Teller (BET) equation by the single point method on the basis of nitrogen uptake at liquid-nitrogen temperature.

The reaction apparatus of BET surface area measurement consisted of two feed lines for helium and nitrogen. The flow rate of the gas was adjusted by means of fine-metering valve on the gas chromatograph. The sample cell made from pyrex glass. The schematic diagram of the reaction apparatus was shown in Figure 4.3.

The mixture gases of helium and nitrogen flowed through the system at the nitrogen relative pressure of 0.3. The catalyst sample (ca. 0.3 to 0.5 g) was placed in the sample cell, which was then heated up to 160^{o}C and held at this temperature for 2 h. After the catalyst sample was cooled down to room temperature, nitrogen uptakes were measured as follows.

Step (1) Adsorption step: The sample that set in the sample cell was dipped into liquid nitrogen. Nitrogen gas that flowed through the system was adsorbed on the surface of the sample until equilibrium was reached.

Step (2) Desorption step: The sample cell with nitrogen gas-adsorbed catalyst sample was dipped into the water at room temperature. The adsorbed nitrogen gas was desorbed from the surface of the sample. This step was completed when the indicator line was in the position of the base line.

Step (3) Calibration step: 1 ml of nitrogen gas at atmospheric pressure was injected through the calibration port of the gas chromatograph and the area was measured. The area was the calibration peak. The calculation method is explained in Appendix C.

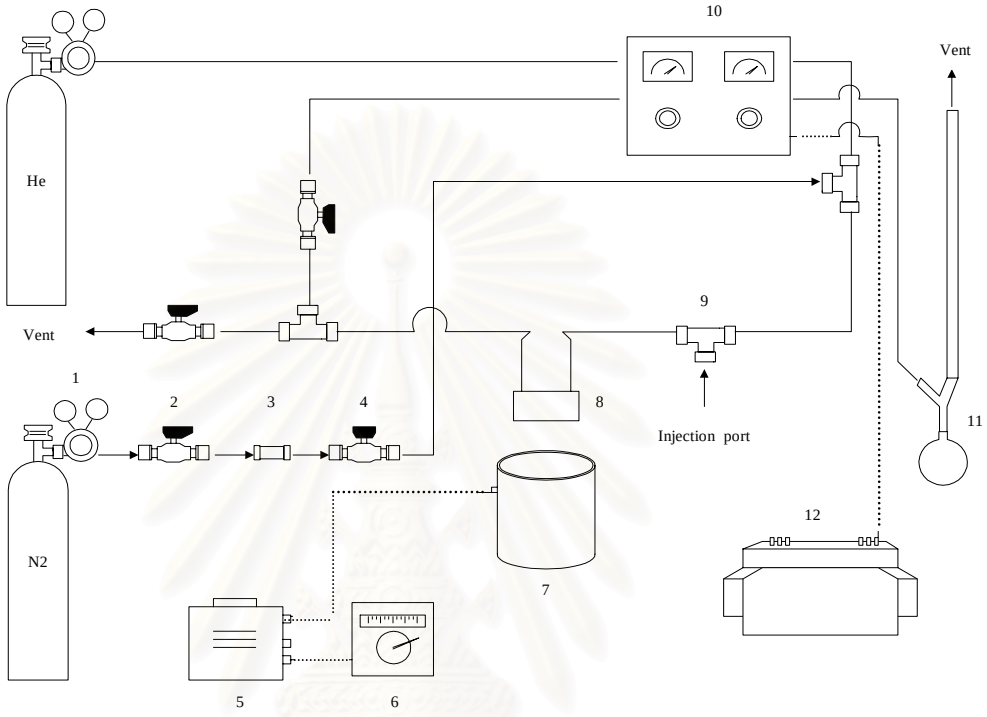

1. Pressure regulator	5. Voltage transformer	9. Three-way valve
2. On-off valve	6. Temperature controller	10. Gas chromatograph with TCD
3. Gas filter	7. Heater	11. Bubble flowmeter
4. Needle valve	8. Sample cell	12. Recorder

Figure 4.3 The schematic diagram of the reaction apparatus of BET surface area measurement.

4.4.4 Infrared Spectroscopy (IR)

The functional group in the samples was determined by using infrared spectroscopy. Before measurement, the sample was mixed with KBr and then was formed into a thin wafer. Acidity of the samples was measured by pyridine adsorption

Model of IR for experiments: Nicolet impact 400 at Center of Excellences on Catalysis and Catalytic Reaction Engineering, Chulalongkorn University.

4.4.5 CO_2-Temperature Programmed Desorption

The basicity of samples was measured by CO_2-TPD technique. The catalyst sample (0.5 g) was placed in the reactor. Procedure is following

Step (1) Preheat step: Sample in reactor was heated in He flow at 400^{o}C and held for 1 h to remove the surface impurities.

Step (2) Adsorption step: The sample was saturated in CO_2 (30 ml/min) at 100^{o}C for 1 h.

Step (3) Desorption step: After saturation, the temperature was increased from 100-400^{o}C at a rate of 10^{o}C/min. The amount of desorbed CO_2 was determined by measuring the area of the desorption profiles.

4.4.6 Electron Spin Resonance Spectroscopy (ESR)

Electron spin configuration was detected by using Electron spin resonance spectroscopy (ESR). The sample was degassed before measurement at room temperature.

Model of Electron spin resonance spectroscopy (ESR) for experiments: JEOL model JES-RE2X at the Sciencetific and Technological Research Equipment Center, Chulalongkorn University (STREC).

CHAPTER V

RESULTS AND DISCUSSION

The effects of type and amount of the second element added in zirconia synthesized by glycothermal method are explained in this chapter.

5.1 Effect of amount of the second element added in zirconia

The second elements selected to study in this research are following: silicon, aluminium, phosphorous, gallium, lead and bismuth. The reasons were described in the part of introduction.

5.1.1 Silicon doped zirconia

Silicon doped zirconia was synthesized from zirconium *tetra-n*-propoxide in 1,4-butanediol at 300 °C for 2 h. Molar ratio of Si/Zr was varied from 0 to 0.02. TEOS was used as source of Si. X-ray diffraction patterns of products with vary molar ratio of Si/Zr were shown in Figure 5.1. Both undoped and silicon doped zirconia obtained only tetragonal phase at all ratio of Si/Zr.

Scanning electron micrograph images of silicon-doped zirconia are shown in Figure 5.2. All the products were composed of spherical particles. The more doping silica resulted in the more agglomerating of secondary particles. Moreover, when compared amount of small secondary particles in an interesting area, the amount of small sizes were mostly contained with doping more silicon. It might suggest that the small amount of silicon would retard a growth of secondary particle apparently in the molar ratio of 0.005, 0.01 and 0.02.

Silica doped zirconia samples were characterized by infrared spectroscopy method. Figure 5.3 illustrates IR spectra of 400 ^{o}C-calcined samples at Si/Zr ratio of 0, 0.002, 0.005, 0.01 and 0.02, respectively. The IR bands can be assigned to the glycol moieties and water at around ~1300 and ~1600 cm^{-1}. Si-O-Zr bond was

observed at around ~1000 cm^{-1} (Yoshida *et al*., 2003) and vibration band shifted higher at high doping ratio (Kongwudthiti *et al*., 2003b). In addition, vibration band at ~800 cm^{-1} can be assigned to Si-O bond. The characteristic band of OH group was observed clearly at around 3400 cm^{-1} (Das *et al*., 2002 and Bokhimi *et al*., 1998). Cerrato *et al*., 1997 suggested that both undissociated H_2O molecules and OH species (dissociated H_2O) may contribute to the saturation of the coordinatively unsaturated sites, which are cationic or anionic terminations produced in the outer layer of the solid. It would seem that increase of silica cause to more OH groups.

Table 5.1 shows the crystallite size and amount of desorbed CO_2 including BET surface area of the products. Crystallite size of zirconia, which calculated by the XRD broadening, was quite equal to crystallite size of doped zirconia at all ratios. The BET surface area increased by doped more silica content. Amount of adsorbed CO_2 over doped zirconia surface increased more than that of pure zirconia and the CO_2 gas was mosty adsorbed at the molar ratio of 0.005. A few authors mentioned (Davydov, 2003 and Cerrato *et al*., 1997) that CO_2 molecules were chemically bonded with basic site, oxygen vacancy site and hydroxyl group over the metal oxide surface. In addition, Wang *et al*. (2001) proposed that surface basic sites might correspond to defects structures. Recently, it has been reported that the CO_2 adsorption over tetragonal zirconia surface can act as bidentate (Manriquez *et al*., 2004) and bicarbonates formed by the interaction between OH groups and CO_2 (Diez *et al*., 2003 and Manriquez *et al*., 2004) and the forms illustrated in Figure 5.4. In agreement with this adsorption behavior, pure zirconia with unclear OH-IR spectrum represented amount of CO_2 adsorption less than doped zirconia having more obvious OH –IR spectra. It might conclude that a number of CO_2 adsorbed sites correspond to hydroxyl groups.

Acidity of undoped and 0.02 Si/Zr samples was characterized by means of irreversible adsorption of pyridine. The nature of acid sites can be defined by a presence of surface protons as the Bronsted sites or cationic centers as the Lewis centre, which are unsaturated in coordination (Davydov, 2003). From IR-pyridine characterization, IR spectra illustrated in Figure 5.5 and vibration signal at

wavelength around ~1450 and 1615 cm^{-1} (Davydov, 2003) identified only bonding of Lewis sites, whereas Bronsted sites (~1540 cm^{-1} (Sohn *et al*., 1996; Davydov, 2003 and Manriquez *et al*., 2004)) was not observed.

To identify defect center of zirconia considerably assumed as existence of Zr^{3+} sites, a spin of unpaired electron was detected by means of ESR. Figure 5.6 shows relative ESR intensity at various ratios of Si/Zr. Zr^{3+} signals represented at $g_{\perp}$~1.97 and $g_{\parallel}$~1.95 that was very close to the positions of Zr^{3+} observed by many researchers reported in Table 5.2. Only $g_{\perp}$~ was considered in this work due to the apparent signal. ESR intensity of undoped zirconia was the highest compared to others and the intensity decreased when silicon added. This owing to a presence of hydroxyl groups combined in a position of coordinatively unsaturated sites resulting in less Zr^{3+} intensity (Zhao *et al*., 2004).

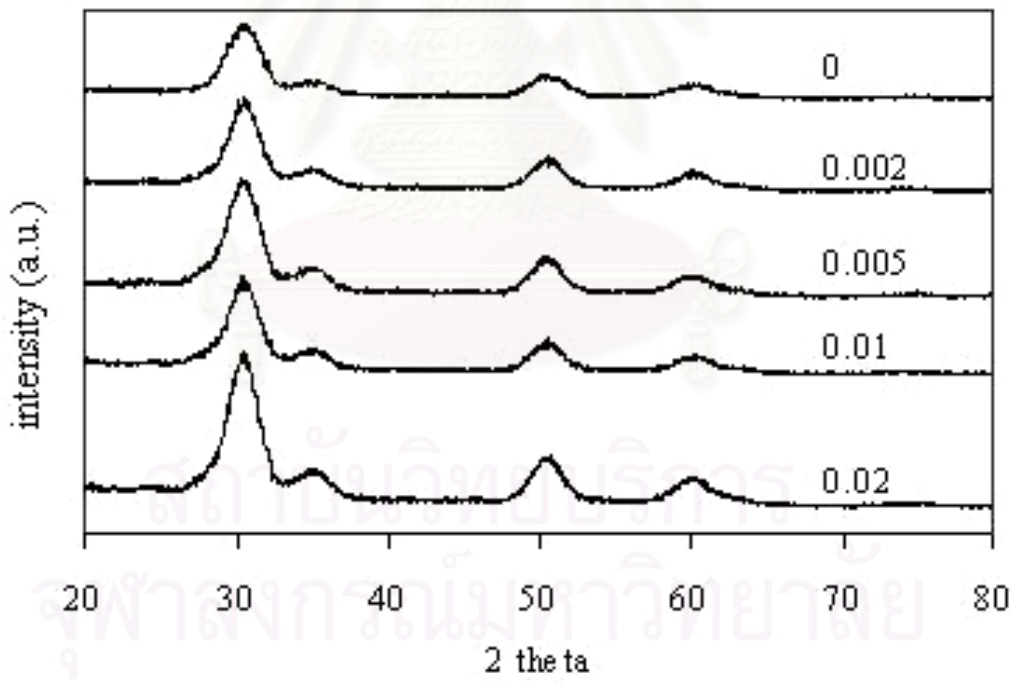

Figure 5.1 The XRD patterns for silicon doped zirconia with various ratio of Si/Zr.

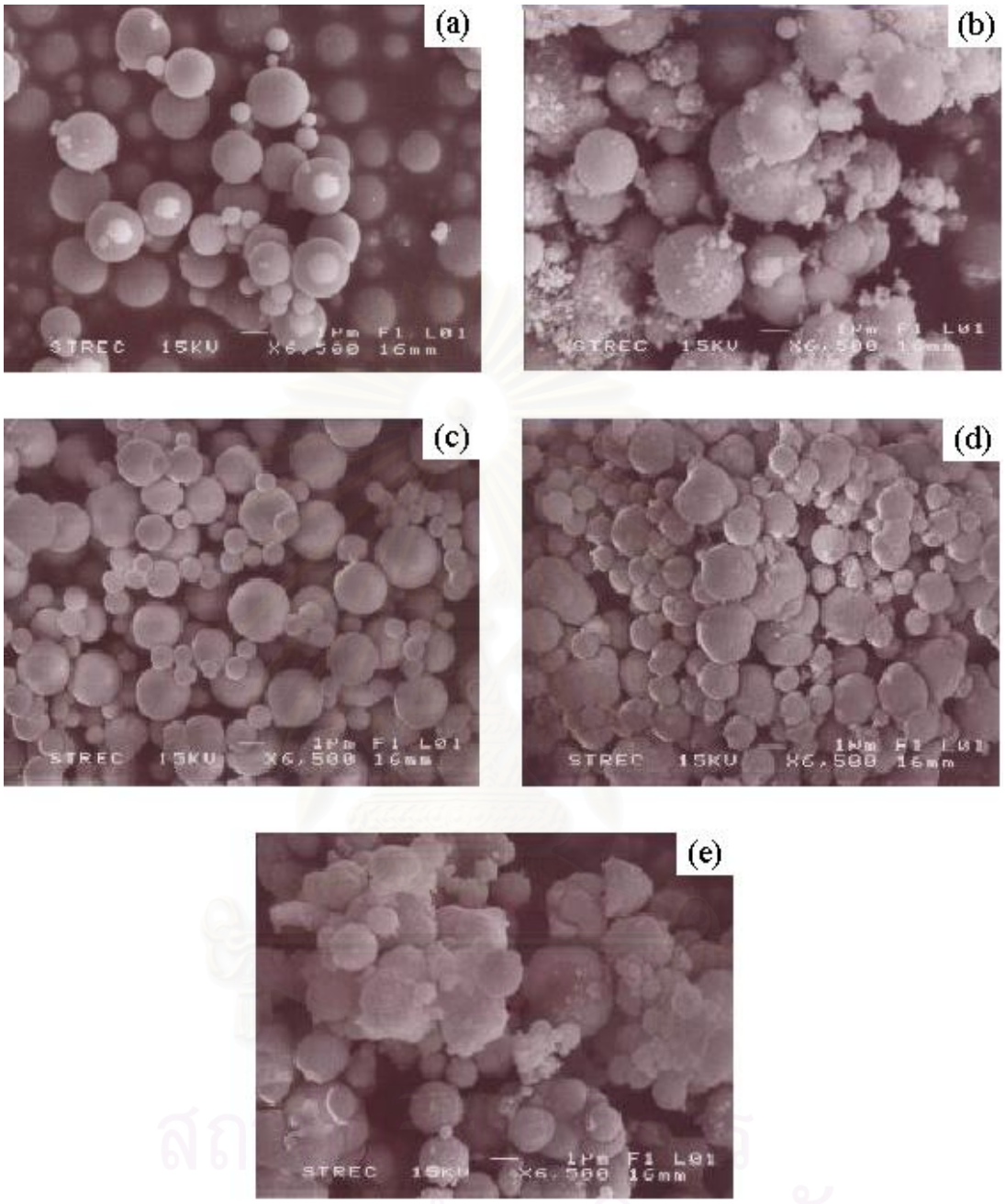

Figure 5.2 Scanning electron micrographs of silicon doped zirconia at Si/Zr ratio (a) 0 (b) 0.002 (c) 0.005 (d) 0.01 and (e) 0.02.

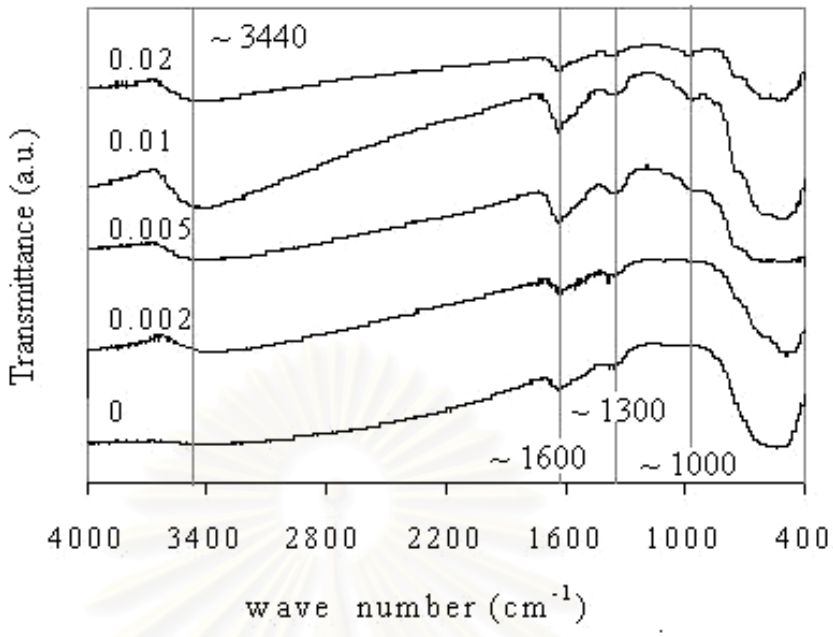

Figure 5.3 IR spectra of silicon doped zirconia at the Si/Zr ratio of 0, 0.002, 0.005, 0.01 and 0.02.

Table 5.1 Crystallite size, BET surface and amount of desorbed CO_2 of silicon doped zirconia synthesized at 300°C for 2 h.

Si/Zr ratio	Crystallite size (nm)	Surface area (m^2/g)	Amount of CO_2 (micromole)
0	3.6	114	27.6
0.002	3.6	120	79.8
0.005	3.4	143	103.4
0.01	3.6	139	77.6
0.02	3.7	132	42.3

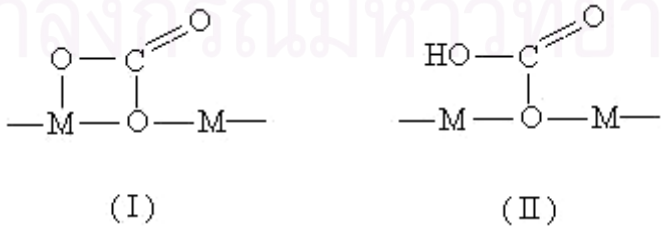

(I) (II)

Figure 5.4 CO_2 coordination on basic sites: (I) bidentated and (II) bicarbonate (Manriquez *et al*., 2004).

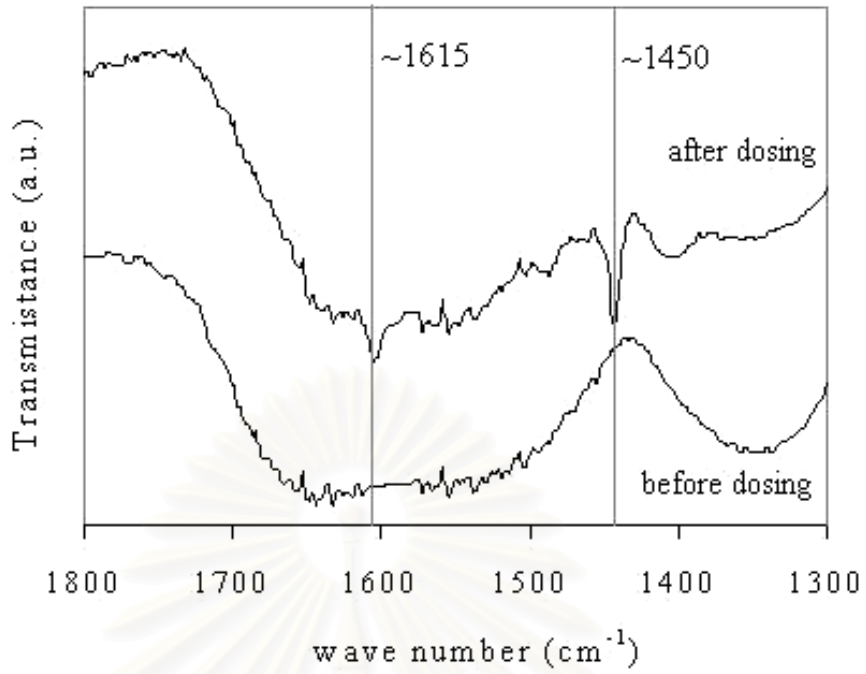

Figure 5.5 IR-pyridine spectra of undoped zirconia.

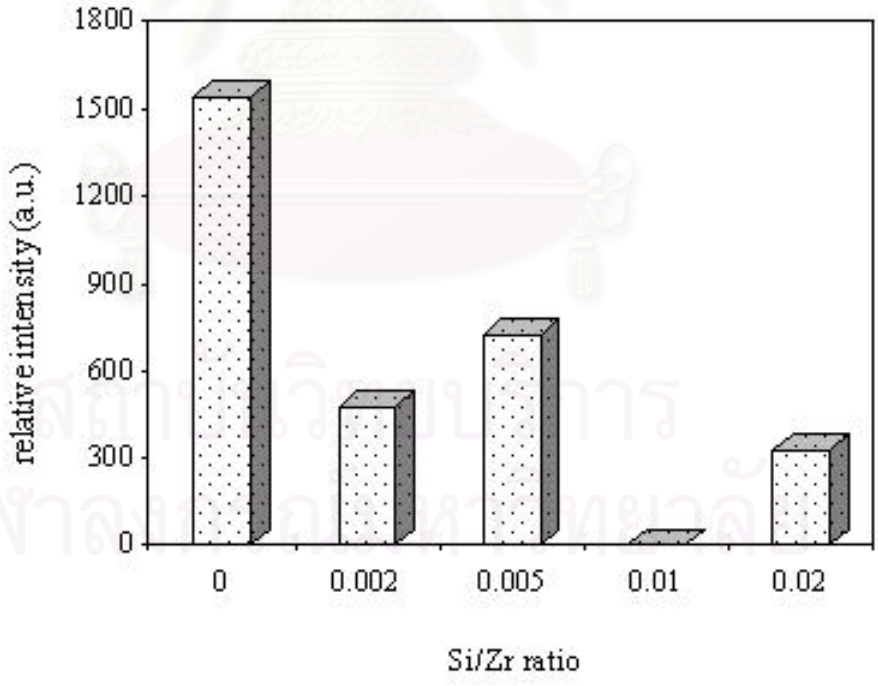

Figure 5.6 Bar diagram shows relative ESR intensity of Si/Zr at various ratios.

Table 5.2 ESR parameters of Zr^{3+} observed in different systems.

Paramagnetic ion	g-value	Reference
Zr^{3+} in ZrO_2	$g_{\parallel} = 1.956$	Torralvo and Alario, 1984
	$g_{\perp} = 1.981$	
Zr^{3+} in ZrO_2	$g_{\parallel} = 1.953$	Moterra *et al*., 1990
	$g_{\perp} = 1.978$	
Zr^{3+} in sulfated zirconia	$g_{\parallel} = 1.951$	Chen *et al*., 1993
	$g_{\perp} = 1.979$	
Zr^{3+} in ZrO_2	$g_{\parallel} = 1.961$	Liu *et al*., 1995
	$g_{\perp} = 1.974$	
Zr^{3+} in V_2O_5/ZrO_2	$g_{\perp} = 1.97$	Adamski *et al*., 1999
Zr^{3+} in sulfated zirconia	$g_{\parallel} = 1.967$	Carlos *et al*., 1999
	$g_{\perp} = 1.982$	
Zr^{3+} in $Pt/WO_x/ZrO_2$	$g_{\parallel} = 1.96$	Punnoose and Seehra, 2002
	$g_{\perp} = 1.98$	
Zr^{3+} in ZrO_2	$g_{\parallel} = 1.957$	Zhao *et al*., 2004
	$g_{\perp} = 1.975$	

5.1.2 Aluminium doped zirconia

To identify phase of doped zirconia, X-ray diffraction technique was used as mentioned in 5.1.1. The XRD patterns of doped zirconia were shown in Figure 5.7. Pure tetragonal was observed at all ratio of Al/Zr.

Figure 5.8 shows scanning electron micrographs images of aluminium doped zirconia. All the products were composed of spherical particles. Comparison to pure zirconia, doping alumina resulted in agglomeration of smaller secondary particle sizes.

Figure 5.9 shows IR spectra of the samples at the Al/Zr ratio of 0.002, 0.005, 0.01 and 0.02, respectively. The IR bands can be assigned to the glycol moieties at around ~1300 and water ~1600 cm^{-1}. The broad peak at ~3400 cm^{-1} is attributed to O-H group stretching vibration of water associated with the oxide. Zr-O-Al bond at ~2100 cm^{-1} cannot observe in our work.

The crystallite size, amount of desorbed CO_2 and BET surface area of the products was shown in Table 5.3. The crystallite sizes of aluminium doped zirconia were smaller than undoped zirconia owing to inhibition of crystal growth by aluminium ions. The BET surface area increased when doped with aluminium. The amount of CO_2 adsorbed for aluminium doped zirconia was higher than that of undoped zirconia. Therefore, basicity of alumina doped zirconia was developed in agreement with result of Moran *et al*. (1999). Doping aluminium, which has lower valence cations, in zirconia matrix leads to increase of the number of oxygen ion vacancies to compensate imbalance charge (Elisabeth *et al.*, 2003).

Intensities of Zr^{3+} paramagnetic in alumina doped zirconia were shown in Figure 5.10. When doped zirconia by aluminium, there was no signal of Zr^{3+} represented at all ratios except at the ratio of 0.005, which can be observed less than undoped zirconia. It might suggest that reduction of Zr^{3+} intensity arises from bonding of dissociated OH group to oxygen vacancies to be fully coordinated of zirconium center.

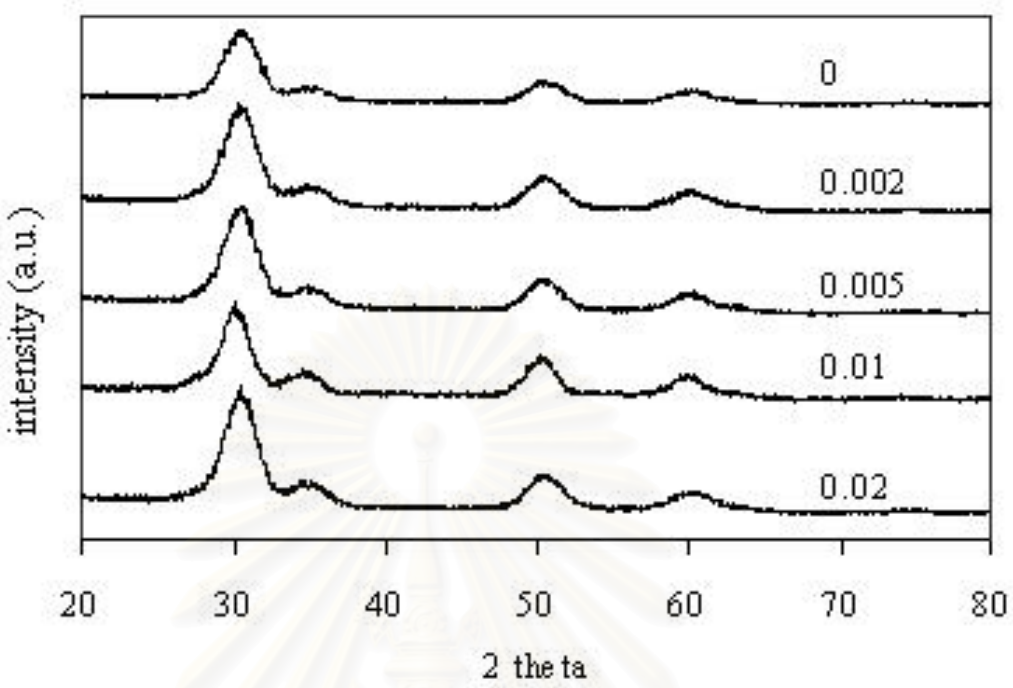

Figure 5.7 The XRD patterns for aluminium doped zirconia with various ratios of Al/Zr.

Table 5.3 Crystallite size, BET surface and amount of desorbed CO_2 of aluminium doped zirconia synthesized at 300°C for 2 h.

Al/Zr ratio	Crystallite size (nm)	Surface area (m^2/g)	Amount of CO_2 (micro mole)
0	3.6	114	27.6
0.002	3.2	99	56.9
0.005	3.3	114	47.2
0.01	3.3	131	86.1
0.02	3.2	121	63.9

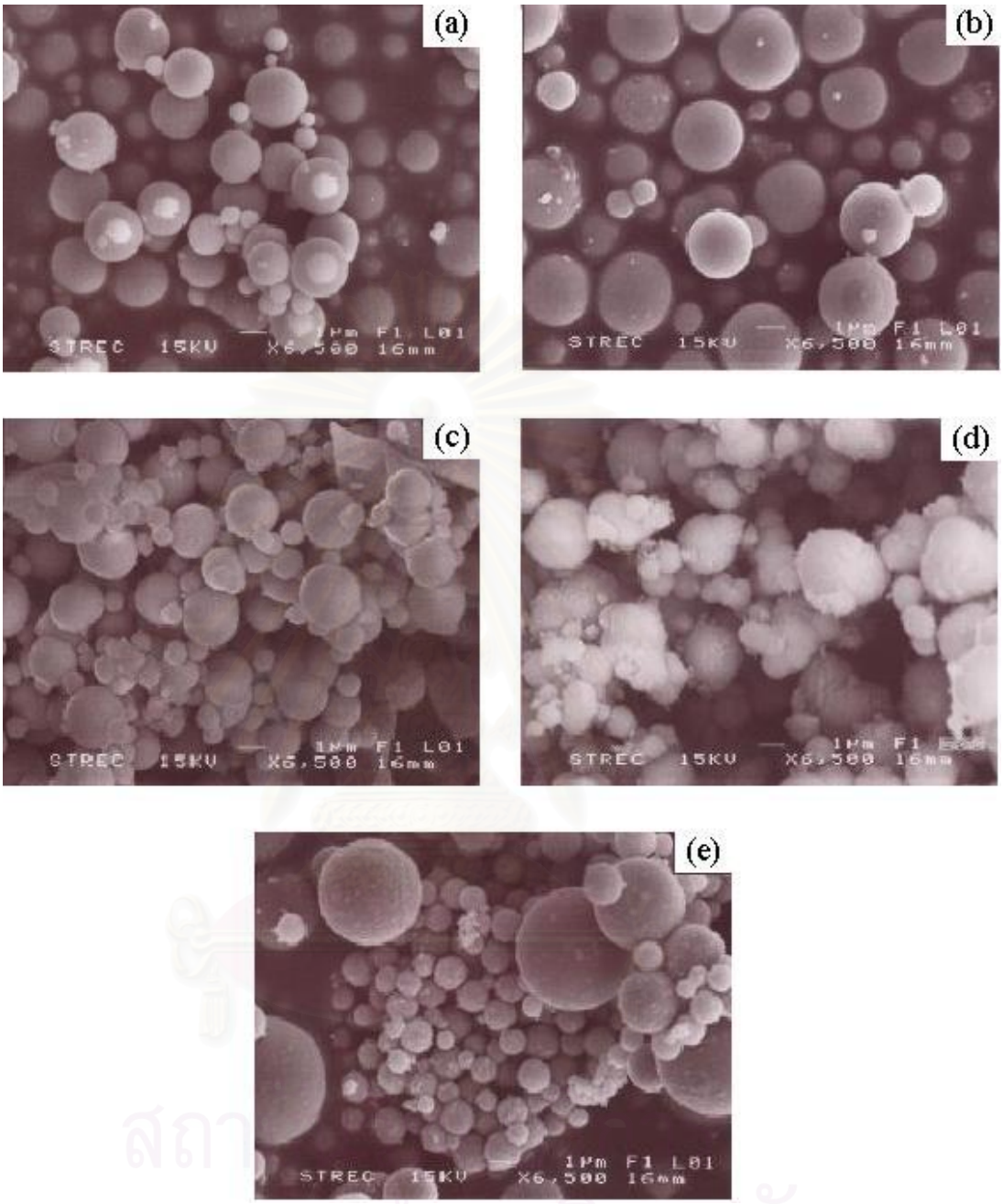

Figure 5.8 Scanning electron micrographs of aluminium doped zirconia at Al/Zr ratio of (a) 0 (b) 0.002 (c) 0.005 (d) 0.01 and (e) 0.02.

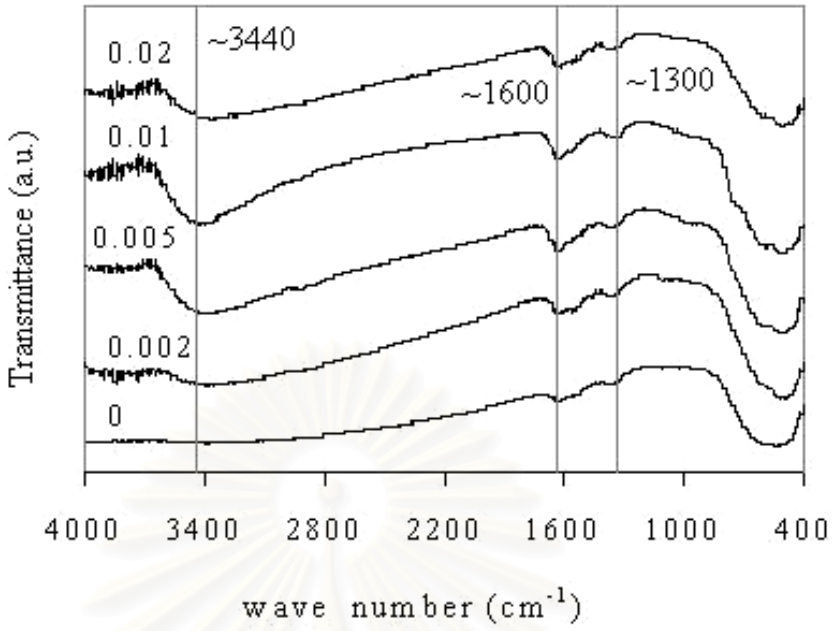

Figure 5.9 IR spectra of aluminium doped zirconia at Al/Zr ratio of 0, 0.002, 0.005, 0.01 and 0.02.

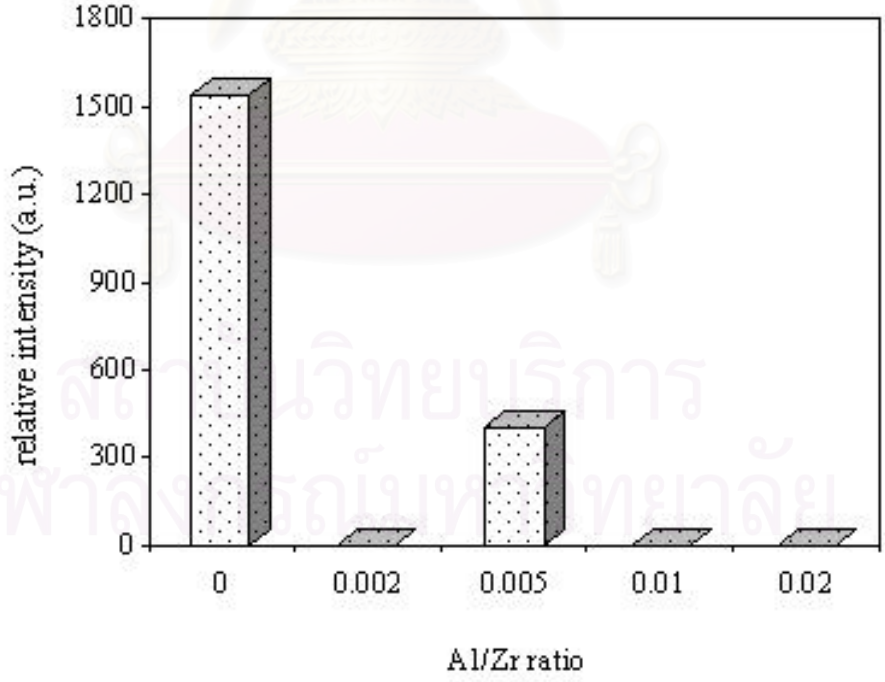

Figure 5.10 Bar diagram shows ESR intensity of Zr^{3+} of Al/Zr at various ratios.

5.1.3 Phosphorous doped zirconia

X-ray diffraction peaks of phosphorous-doped zirconia were shown in Figure 5.11. Phase of phosphorous-doped zirconia were tetragonal similar to all zirconia previously mentioned. Morphology of phosphorous-doped zirconia was shown in Figure 5.12. The secondary particle seems to be very small at high ratio of P/Zr and different from the previous zirconia doped with silicon and aluminium. It seems that phosphorous ions retard agglomeration of primary particle more obviously than silicon or aluminium ions. However, surface area of phosphorous-modified zirconia was not much improved as shown in Table 5.4. Surface area increased more than pure zirconia and not change with amount of phosphorous. Amount of CO_2 on surface area for pure zirconia was higher than that the ratio of 0.005 P/Zr but less than other higher ratio.

The IR spectra of phosphorous-doped zirconia at various ratios were shown in Figure 5.13. The IR bands can be assigned to the glycol moieties and water at around ~1300 and ~1600 cm^{-1}, respectively. The characteristic band of OH group can be observed clearly around 3400 cm^{-1} for doped zirconia. As seen in the result of silicon and alumina-doped zirconia, appearance of hydroxyl group was shown more clearly than pure zirconia.

CO_2 temperature programmed desorption results were reported in Table 5.4. In agreement with silicon and aluminium-doped zirconia, the amount of CO_2 desorption over phosphorous-doped zirconia corresponded to OH groups identified by means of IR spectroscopy directly.

The crystallite sizes of doped zirconia were similar to undoped zirconia. This is because quantity of dopant at each ratio was very small and it could result in a same certain rate of crystal growth.

Figure 5.14 shows Zr^{3+} intensity of zirconia at various ratios of P/Zr. Zr^{3+} intensity was reduced after adding more phosphorous and the intensity correlated to hydroxyl group as mentioned in 5.1.1 and 5.1.2. Compared to undoped zirconia, the

amount of Zr^{3+} was decreased by doping more phosphorous, on the contrary hydroxyl groups were increased.

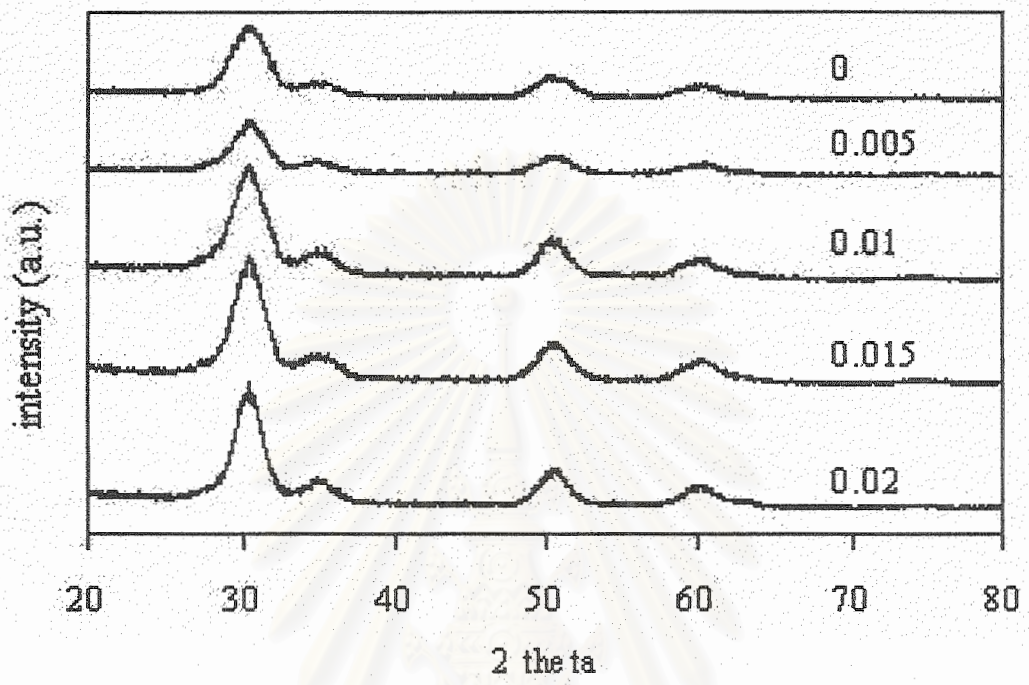

Figure 5.11 The XRD patterns for phosphorous doped zirconia with various ratio of P/Zr.

Table 5.4 Crystallite size, BET surface and amount of desorbed CO_2 of phosphorous doped zirconia synthesized at 300°C for 2 h.

P/Zr ratio	Crystallite size (nm)	Surface area (m^2/g)	Amount of CO_2 (micro mole)
0	3.6	114	27.6
0.005	3.5	120	21.8
0.01	4.0	138	51.8
0.015	3.6	137	48.6
0.02	4.1	138	52.7

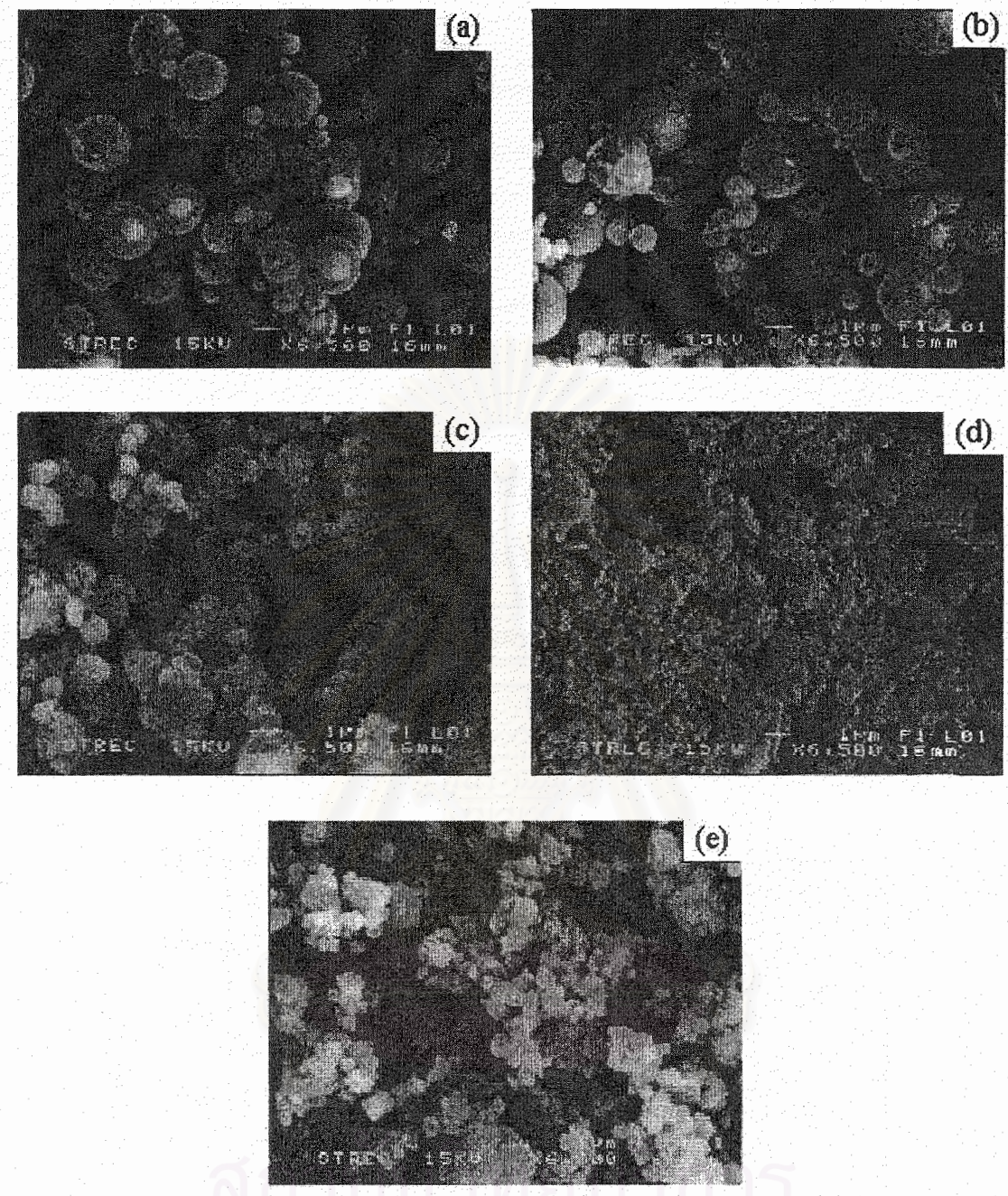

Figure 5.12 Scanning electron micrographs of phosphorous doped zirconia at P/Zr ratio of (a) 0 (b) 0.005 (c) 0.01 (d) 0.015 and (e) 0.02.

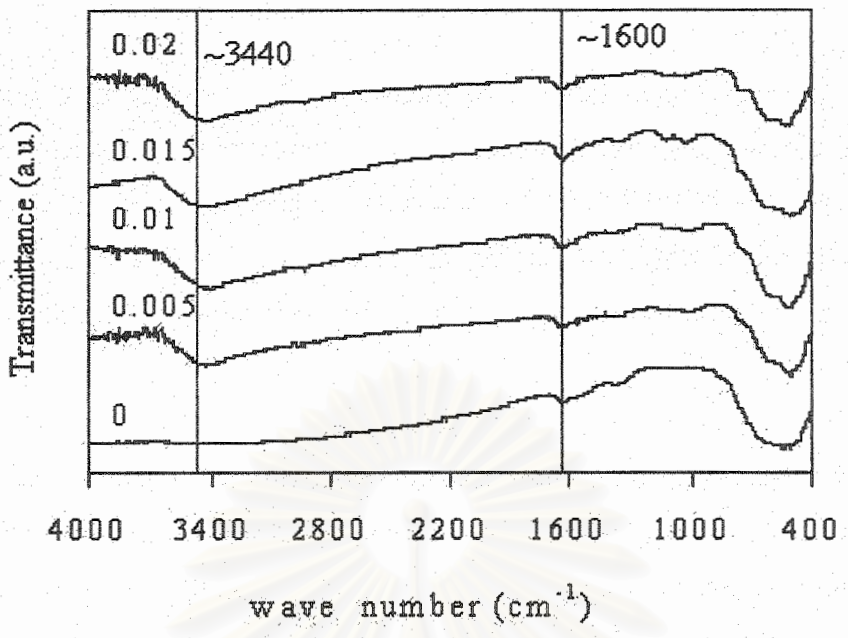

Figure 5.13 IR spectra of phosphorous doped zirconia at the P/Zr ratio of 0, 0.002, 0.005, 0.01 and 0.02.

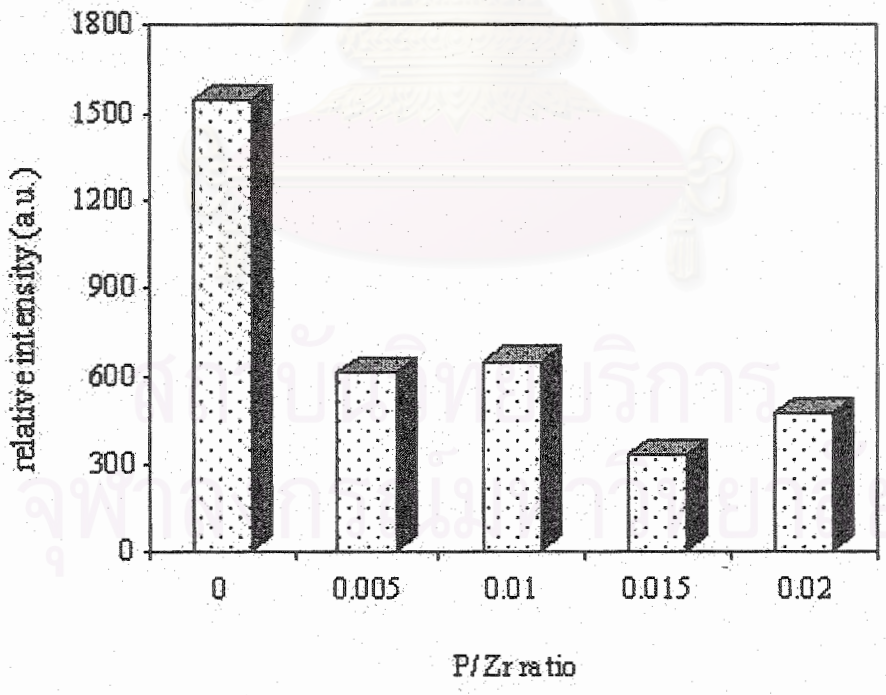

Figure 5.14 Bar diagram shows relative ESR intensity of P/Zr at various ratios.

5.1.4 Gallium doped zirconia

Figure 5.15 shows the XRD pattern of gallium doped zirconia at various ratios. Pure tetragonal was obtained for both doped and undoped zirconia. The X-ray diffraction results were described as in section 5.1.1-5.1.3. SEM images of gallium doped zirconia were shown in Figure 5.16 and we observed uniform size of secondary particles, which were smaller than pure zirconia. It can be discussed as in section 5.1.1-5.1.3.

The IR spectra of gallium doped zirconia were shown in Figure 5.17. The IR bands can be assigned to the glycol moieties and water at around ~1300 and ~1600 cm^{-1}, respectively. The characteristic band of OH group can be observed clearly around 3400 cm^{-1}. In agreement with section 5.1.1-5.1.3, the number of hydroxyl groups over gallium doped zirconia surface was increased compared to pure zirconia.

The crystallite size, amount of desorbed CO_2 and BET surface of gallium doped zirconia were summarized in Table 5.5. Crystallite size and surface area of gallium doped zirconia were less than undoped zirconia while amount of CO_2 at 0.005 Ga/Zr ratio was higher than the other ratios. Similarly, it might be discussed as doping aluminium. Doping gallium might cause to occurrence of oxygen vacancies and dissociated OH groups might bond to the vacancies to be fully coordinated of zirconium center. As shown in Figure 5.17, existence of hydroxyl groups over gallium doped zirconia was more obvious than over pure zirconia.

In addition, there was a relation of hydroxyl groups and Zr^{3+} intensity as described in section 5.1.1-5.1.3. Zr^{3+} intensity of gallium doped zirconia at various ratios were shown in Figure 5.18. Small amount of gallium added in zirconia effect to decrease of intensity.

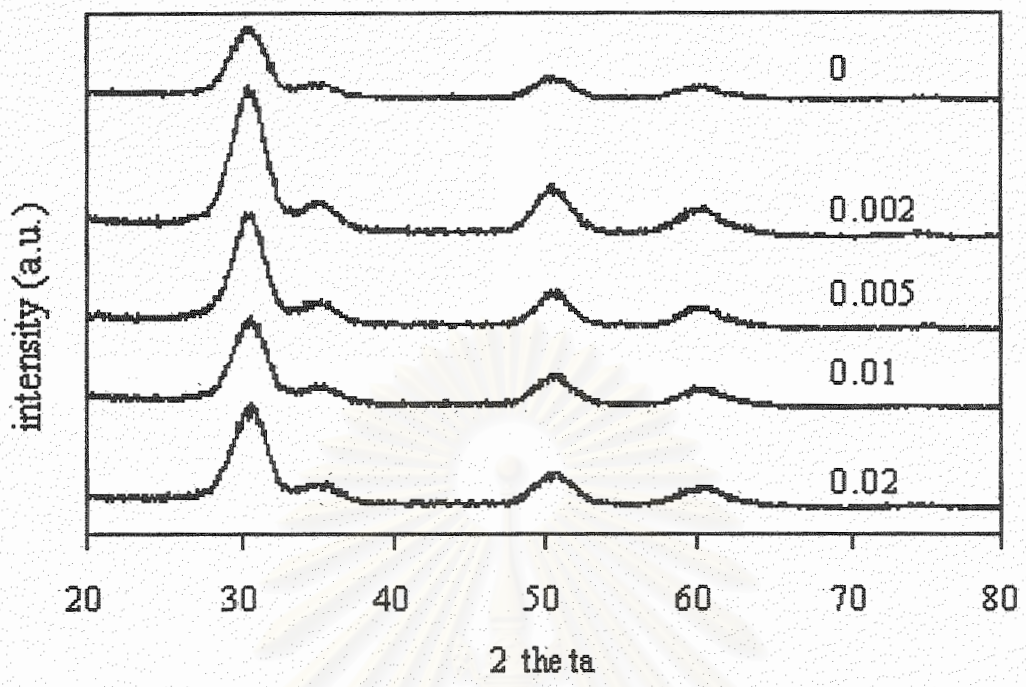

Figure 5.15 The XRD patterns for gallium doped zirconia with various ratio of Ga/Zr.

Table 5.5 Crystallite size, BET surface and amount of desorbed CO_2 of gallium doped zirconia synthesized at 300°C for 2 h.

Ga/Zr ratio	Crystallite size (nm)	Surface area (m^2/g)	Amount of CO_2 (micro mole)
0	3.6	114	27.6
0.002	3	41	23.8
0.005	3.5	105	68.9
0.01	3.3	67	24.8
0.02	3.1	87	26.4

Table 5.5 Crystallite size, BET surface and amount of desorbed CO_2 of gallium doped zirconia synthesized at 300°C for 2 h.

Ga/Zr ratio	Crystallite size (nm)	Surface area (m^2/g)	Amount of CO_2 (micro mole)
0	3.6	114	27.6
0.002	3	41	23.8
0.005	3.5	105	68.9
0.01	3.3	67	24.8
0.02	3.1	87	26.4

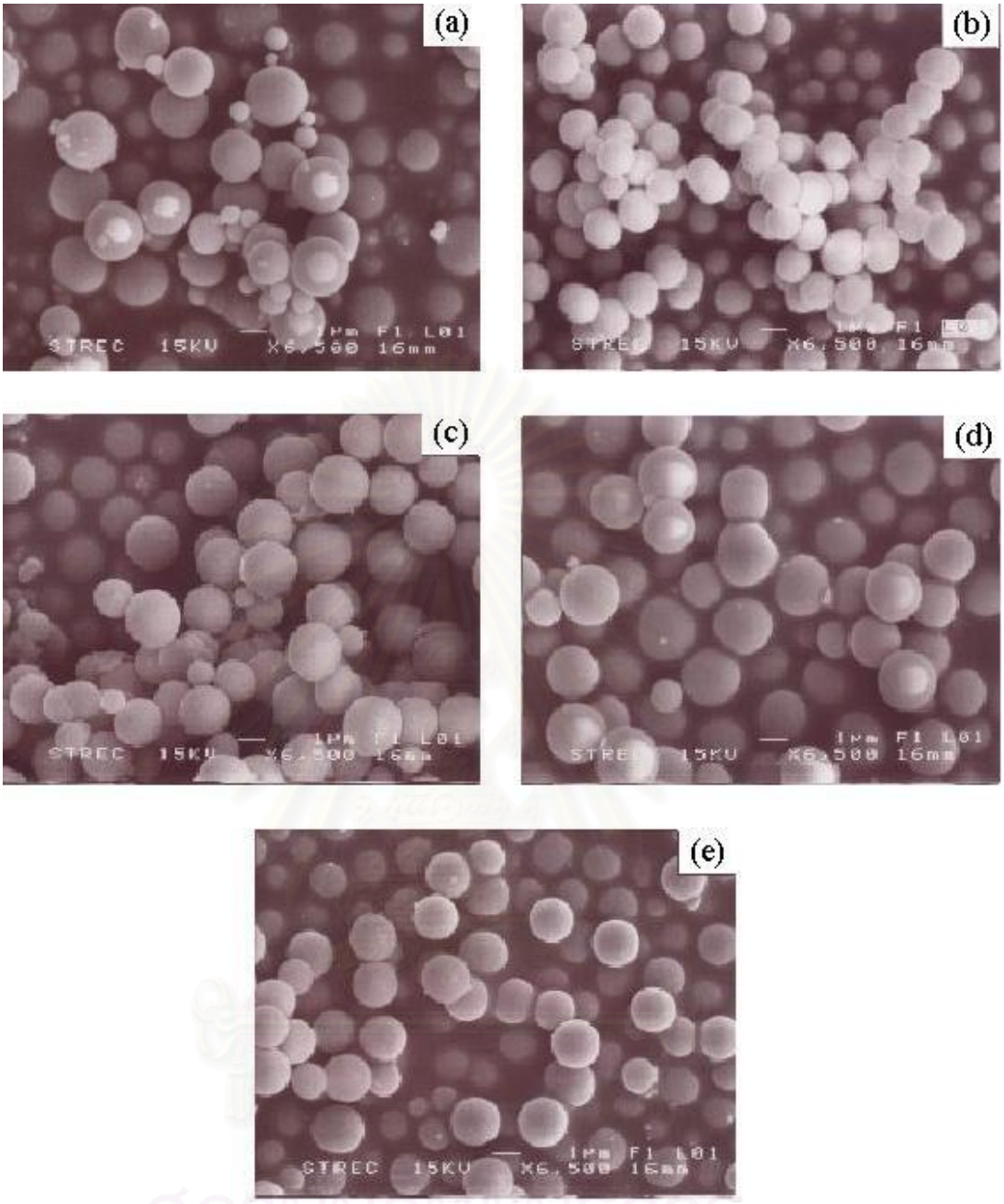

Figure 5.16 Scanning electron micrographs of gallium doped zirconia at Ga/Zr ratio of (a) 0 (b) 0.005 (c) 0.01 (d) 0.015 and (e) 0.02.

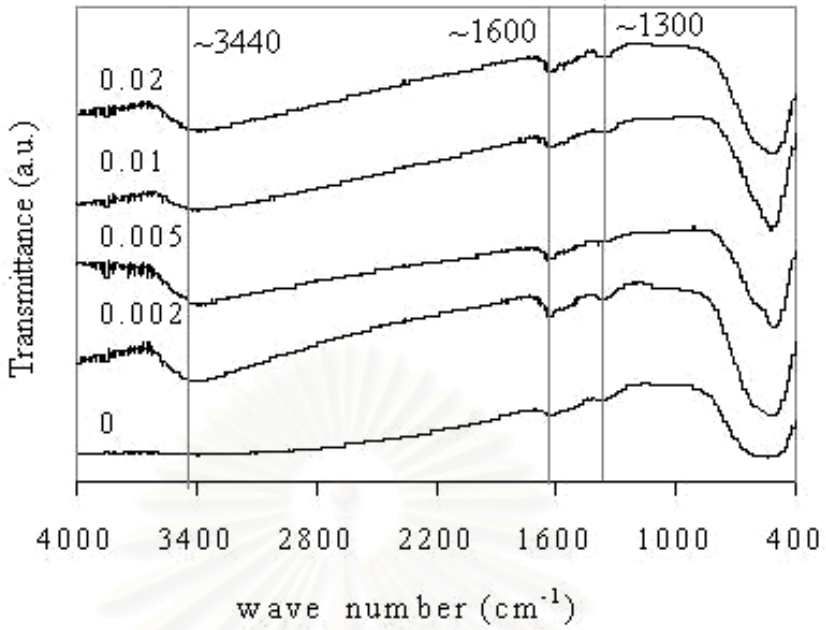

Figure 5.17 IR spectra of the gallium doped zirconia at the Ga/Zr ratio of 0, 0.002, 0.005, 0.01 and 0.02.

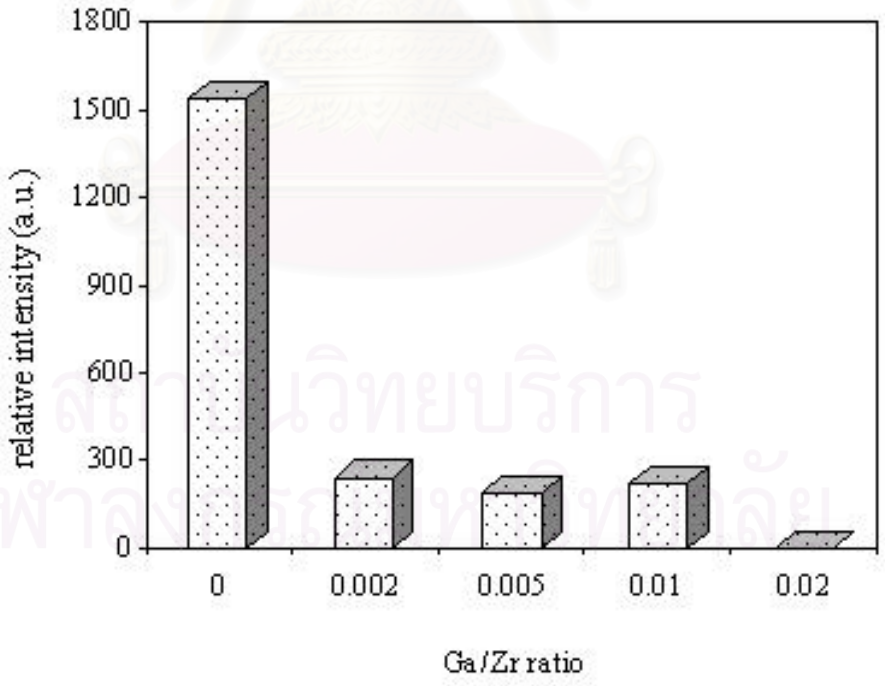

Figure 5.18 Bar diagram shows relative ESR intensity of Ga/Zr at various ratios.

5.1.5 Lead doped zirconia

The XRD pattern of lead doped zirconia at various ratios was shown in Figure 5.19 and the XRD results can be described as in section 5.1.1-5.1.4. Figure 5.20 shows the scanning electron micrographs of lead doped zirconia at various ratio of Pb/Zr. The uniform spherical shape was obtained. Referring to section 5.1.1-5.1.4, it can propose that the second metal ions retard growth rate of secondary particles. In this section, we also found the particle sizes at various Pb/Zr ratios smaller than pure zirconia. Small amount of lead ions might inhibit agglomeration of primary particle resulting in the smaller spherical secondary particles. However, BET surface areas of lead-doped zirconia were extremely decreased compared to other dopants. Doping lead in zirconia matrix might increase density of bulk zirconia.

The IR spectra of lead doped zirconia were shown in Figure 5.21. The IR bands can be assigned to the glycol moieties and water at around ~1300 and ~1600 cm^{-1}, respectively. The characteristic band of OH group can be observed around 3400 cm^{-1} for undoped and doped zirconia.

Table 5.6 exhibits crystallite sizes, amount of desorbed CO_2 and BET surface of lead doped zirconia. Crystallite sizes of lead doped zirconia do not significantly differ and seem to be smaller than pure zirconia. Owing to very low surface area of the zirconia, a tiny OH group signal of IR spectra and very low CO_2 desorption was exhibited in Figure 5.21 and Table 5.6. On the contrary, Zr^{3+} intensities of lead doped zirconia were lower and higher than pure zirconia as shown in Table 5.22. However, the results show that Zr^{3+} intensity decreased when adding lead at 0.002 and 0.005 ratios and increased at 0.01 and 0.02 ratios.

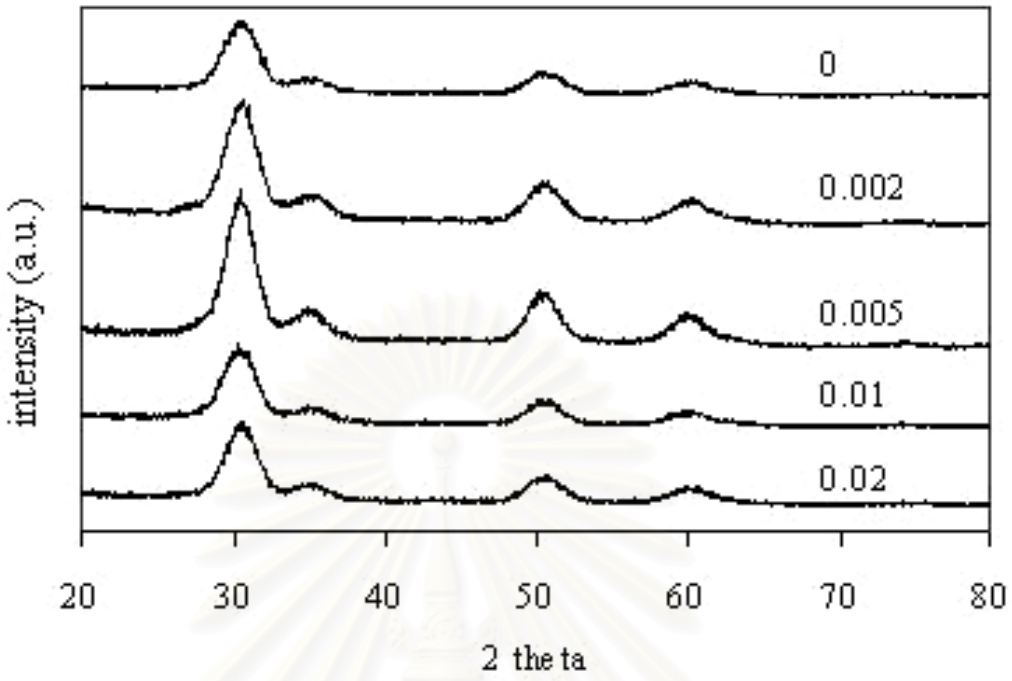

Figure 5.19 The XRD patterns for lead doped zirconia with various ratio of Pb/Zr.

Table 5.6 Crystallite size, BET surface and amount of desorbed CO_2 of lead doped zirconia synthesized at 300°C for 2 h.

Pb/Zr ratio	Crystallite size (nm)	Surface area (m^2/g)	Amount of CO_2 (micro mole)
0	3.6	114	27.6
0.002	3.4	79	28.0
0.005	4.0	58	28.5
0.01	3.1	1	0.0
0.02	3.3	2	0.0

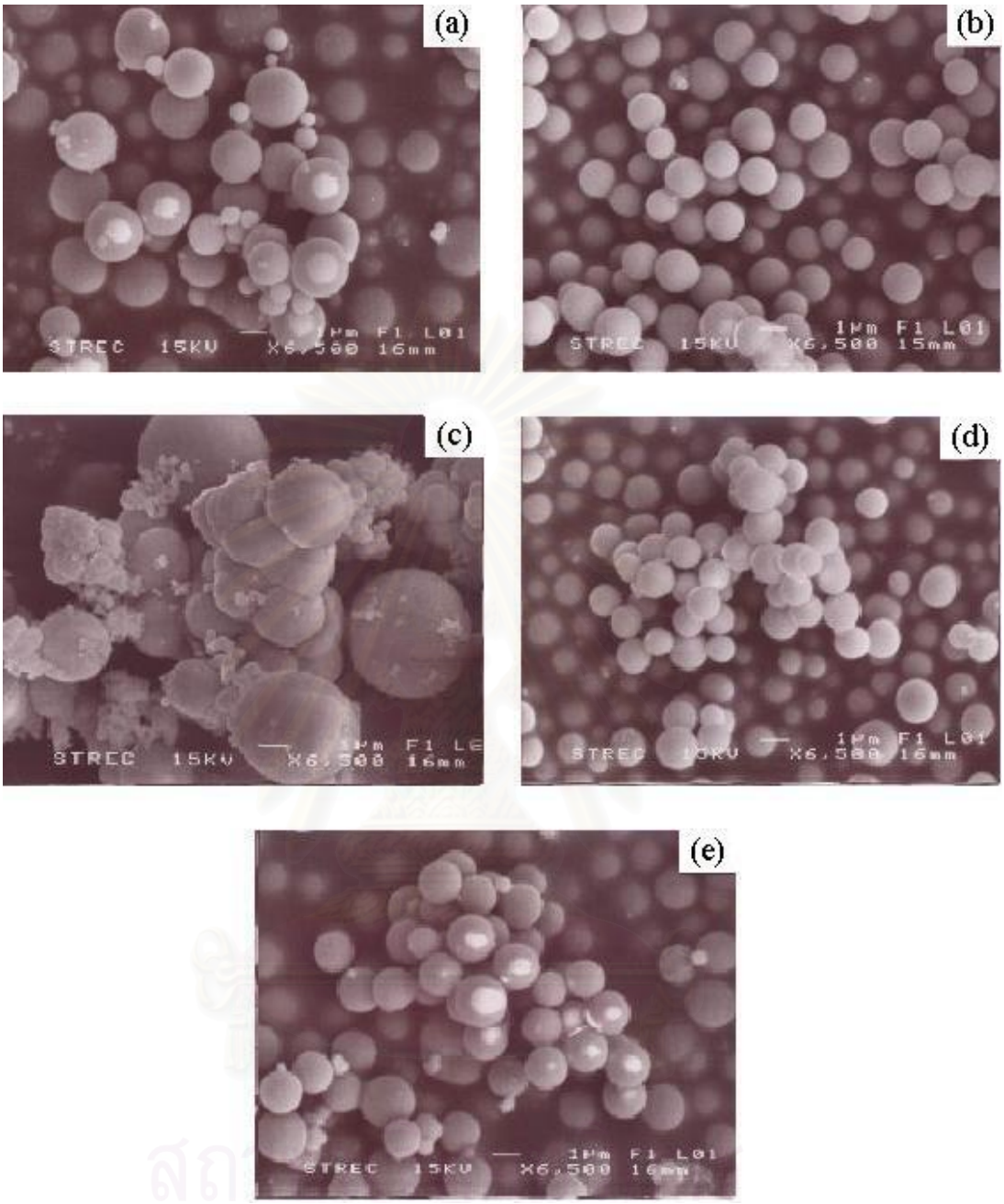

Figure 5.20 Scanning electron micrographs of lead doped zirconia at ratio of Pb/Zr (a) 0 (b) 0.002 (c) 0.005 (d) 0.01 and (e) 0.02.

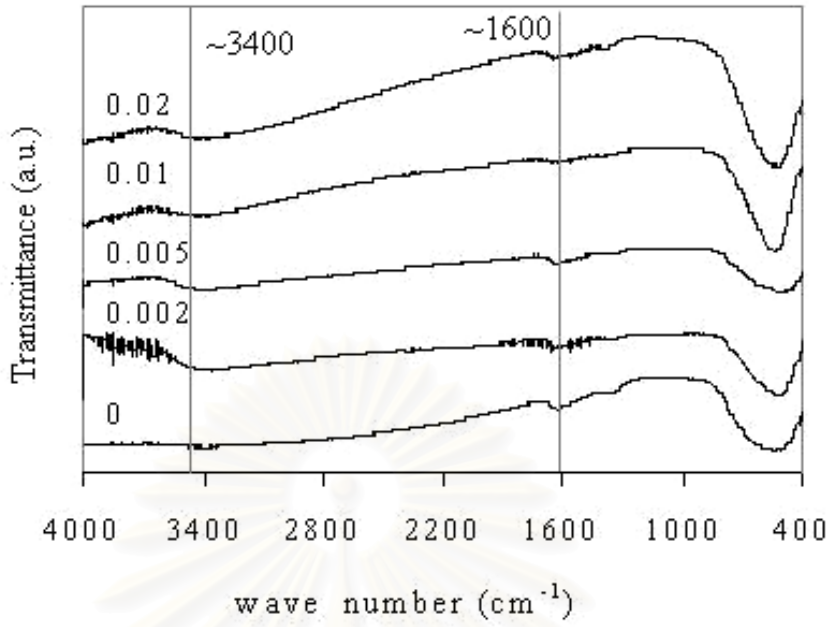

Figure 5.21 IR spectra of lead doped zirconia at the Pb/Zr ratio of 0, 0.002, 0.005, 0.01 and 0.02.

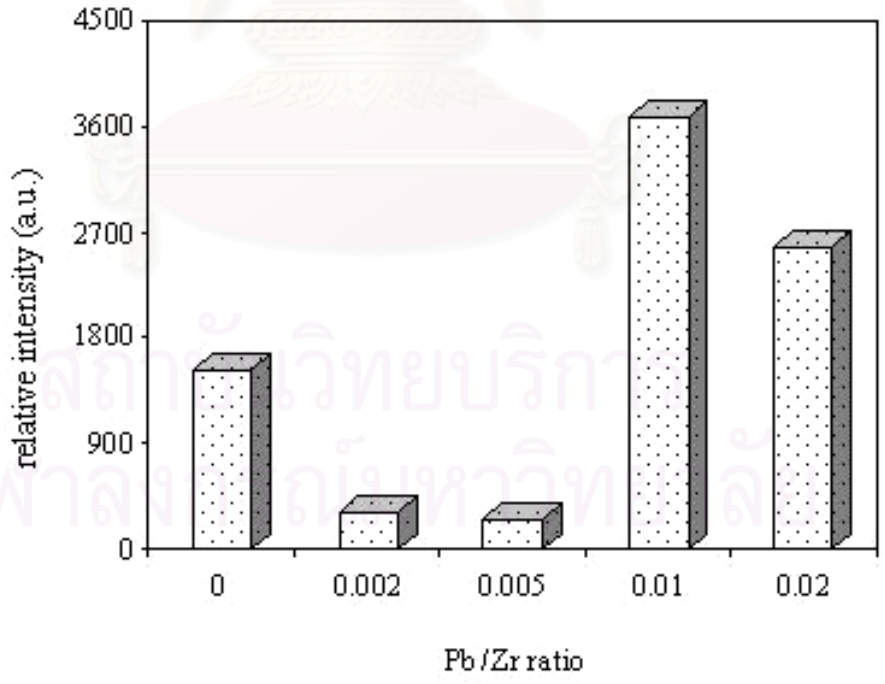

Figure 5.22 Bar diagram shows relative ESR intensity of Pb/Zr at various ratios.

5.1.6 Bismuth doped zirconia

Figure 5.23 show the XRD patterns for bismuth doped zirconia at various ratios of Bi/Zr. All of bismuth-doped zirconia contained a major of tetragonal phase and a minor of monoclinic phase apparently at higher ratio. This might be due to lower valency and larger size of bismuth atomic ion in comparison with Zr^{4+} (Bi^{3+} 1.11 Å and Zr^{4+} 0.84 Å for eight coordination number), which lead to instability in the lattice at lower temperatures and some of tetragonal change to be more thermodynamically stable polymorphs; monoclinic phase. This result was agreement with Jagadish *et al*. (2003) who studied in tin-doped zirconia.

Figure 5.24 shows the scanning electron micrographs of bismuth-doped zirconia at various ratios. The shape of product was spherical, uniform and smaller than undoped zirconia same as mention in section 5.1.1-5.1.5.

The IR spectra of bismuth-doped zirconia were shown in Figure 5.25. The IR bands can be assigned to the glycol moieties and water at around ~1300 and ~1600 cm^{-1}, respectively. The characteristic band of OH groups can be observed ambiguously around 3400 cm^{-1} for both undoped and doped zirconia.

Crystallite size, amount of desorbed CO_2 and BET surface of bismuth doped zirconia were summarized in Table 5.7. Doping zirconia with bismuth seems to affect on small crystallite size because Bi atom might insert in a crystal structure of zirconia and it would retard crystal growth rate. Adding small amount of Bi affected on decreasing surface area remarkably that might be discussed as in section 5.1.5. Moreover, it was reported that very low surface area brought about very low area of CO_2 adsorption profiles and small amount of desorbed CO_2, consequently.

ESR study was shown in Figure 5.26. Bismuth doped zirconia affect on Zr^{3+} intensity higher than undoped zirconia. This indicates that adding bismuth (III) with lower valence and larger size generates lots of oxygen vacancies. Hence, Zr^{4+} ions, which are adjacent to oxygen vacancies, might trap lone pair electrons and result to formation of Zr^{3+}. This result is in agreement with a result obtained by Zhao *et al*.

(2004), who reported the formation of Zr^{3+} might be associated with the removal of hydroxyl group. This can conclude that Zr^{3+} must be the oxygen coordinatively unsaturated zirconium.

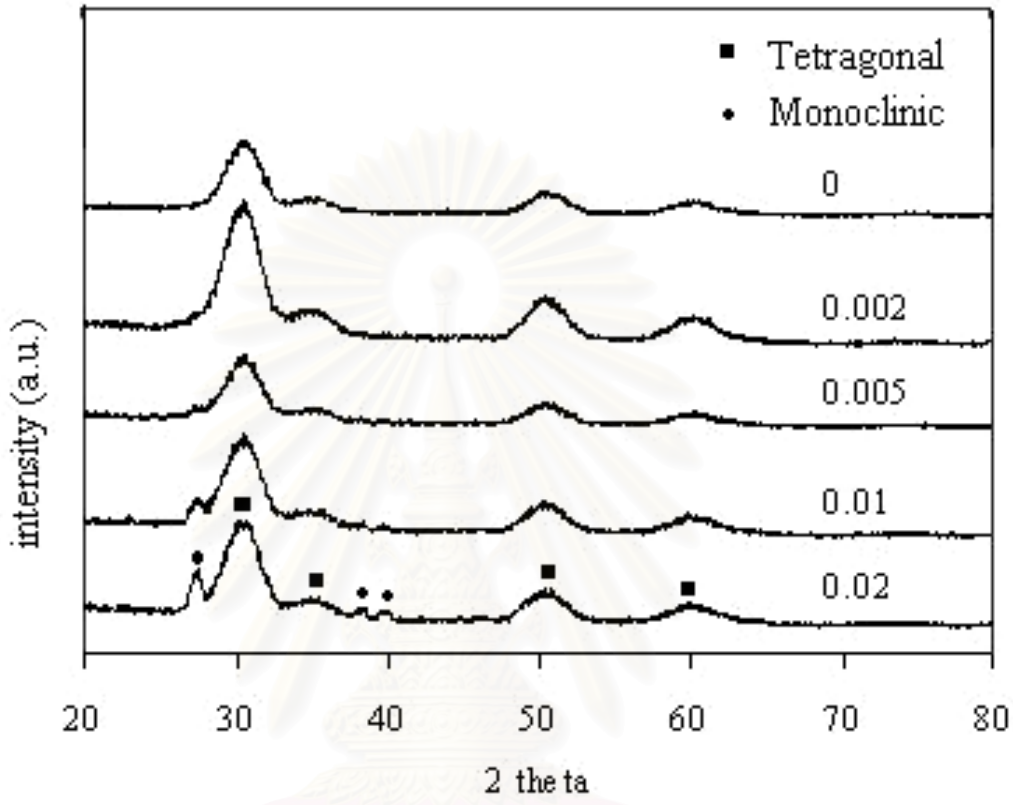

Figure 5.23 The XRD patterns for bismuth doped zirconia with various ratio of Bi/Zr.

Table 5.7 Crystallite size, BET surface and amount of desorbed CO_2 of bismuth doped zirconia synthesized at 300°C for 2 h.

Bi/Zr ratio	Crystallite size (nm)	Surface area (m^2/g)	Amount of CO_2 (micro mole)
0	3.6	114	27.6
0.002	3.0	3	2.7
0.005	3.4	29	16.4
0.01	2.9	3	9.2
0.02	3.1	34	22.6

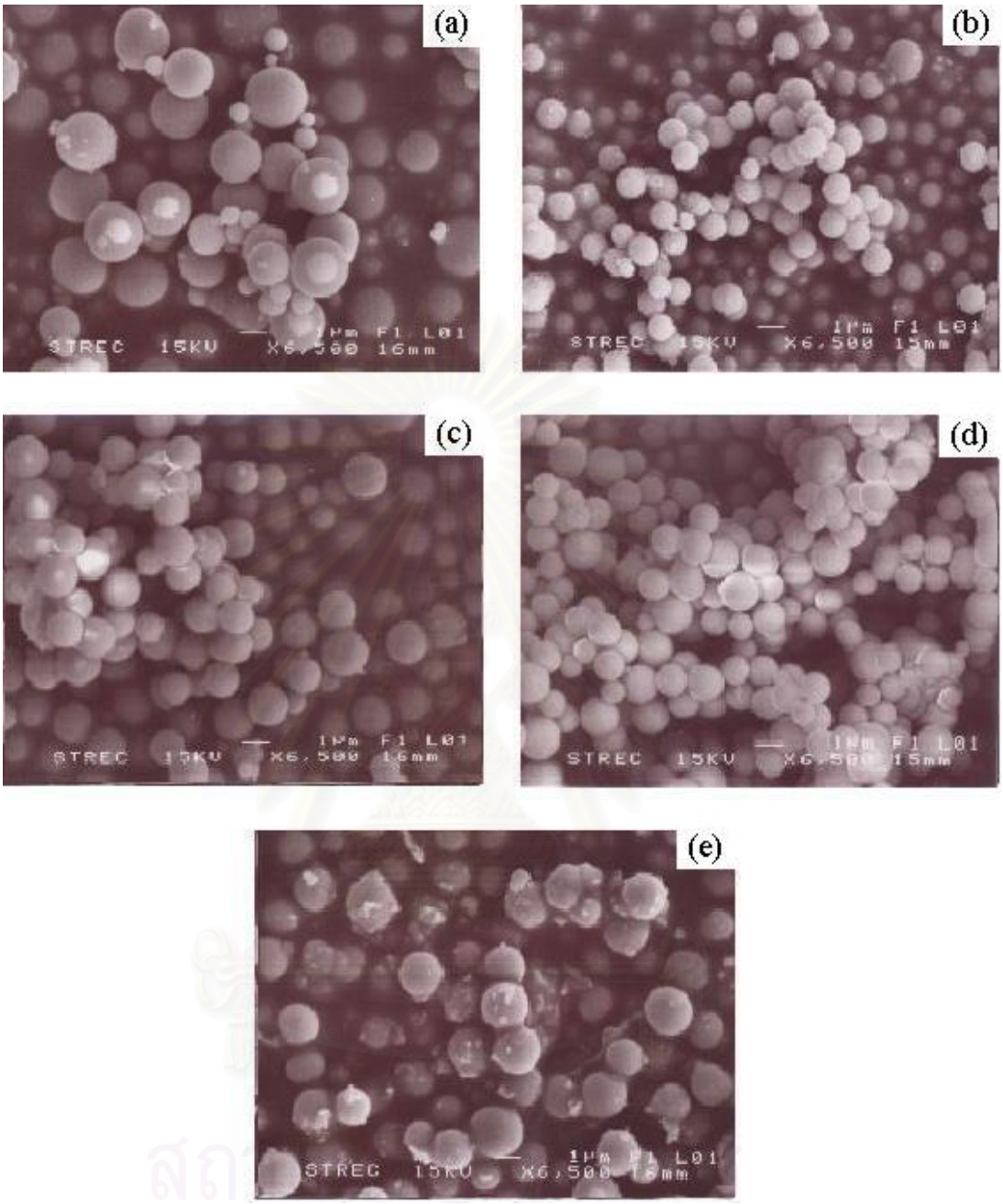

Figure 5.24 Scanning electron micrographs of bismuth doped zirconia at ratio of Bi/Zr (a) 0 (b) 0.002 (c) 0.005 (d) 0.01 and (e) 0.02.

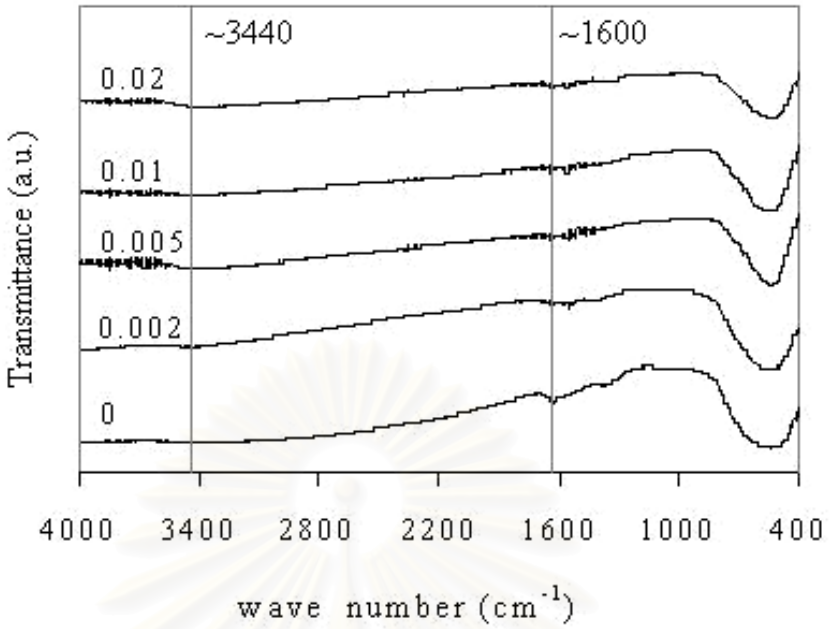

Figure 5.25 IR spectra of bismuth doped zirconia at the Bi/Zr ratio of 0, 0.002, 0.005, 0.01 and 0.02.

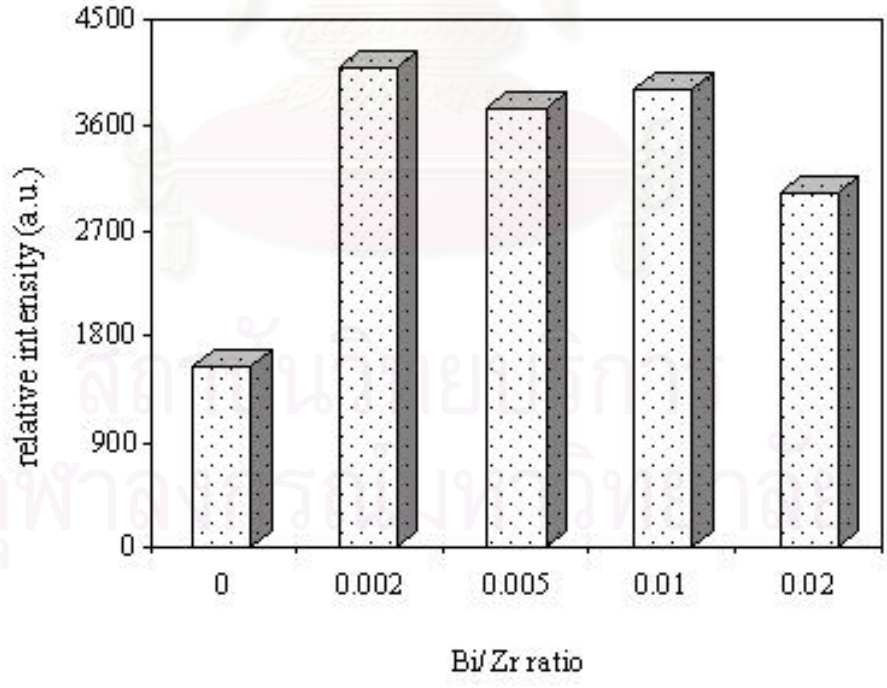

Figure 5.26 Bar diagram to show relative intensity ESR of Bi/Zr at various ratios.

5.2 Effect of types of the second element added in zirconia

From the results mentioned above, we consider ionic size effect of dopant. The sizes were arranged from large to small as following, Bi > Pb > Zr > Ga > Al > Si > P (1.17, 0.94, 0.84, 0.62, 0.54, 0.4 and 0.38 Å, respectively (Aylward *et al*., 2002)). The XRD pattern of second-metal doped zirconia affected slightly on phase structure and shows in Figure 5.27. Undoped zirconia and doping zirconia with Si, Al, P, Ga and Pb exhibited pure tetragonal phase, while Bi added in zirconia showed an appearance of monoclinic phase as discussed in section 5.1.6. Although sizes of Bi and Pb ions are larger than Zr ions, adding lead was not effect on existence of monoclinic phase unlike bismuth because ionic size of Pb ions are close to Zr ion.

Ex-situ IR spectroscopy results showed that adding the second element made hydroxyl groups appeared, however, it was observed very small amount of hydroxyl groups by adding Bi and Pb ions. These IR results indicate that adding dopant can modify surface chemistry by forming hydroxyl group.

In addition, adding dopant with smaller size of dopant (Si, Al, P, Ga) had no significant effect on crystallite size and preserved surface area, whereas adding Bi and Pb ion, crystallite size seem smaller than pure zirconia, on the other hand, affected on decreasing markedly of specific surface area when compared to other dopant.

From ESR characterization, intensity of Zr^{3+} of doping zirconia by bismuth and lead were very high although they resulted in very low surface areas. Decreasing of Zr^{3+} intensity can be attributed to bonding of oxygen atom in OH group to the coordinatively unsaturated Zr sites.

The number of surface hydroxyl groups and CO_2 desorption can be improved by adding the second element as Si, Al, P and Ga. However, the intensity of Zr^{3+} was in contrast with a presence of OH group. On the other hand, when doped zirconia by Pb and Bi, existence of hydroxyl group correlated to amount of CO_2 desorption was decreased because of very low surface area arising from densification of zirconia matrix.

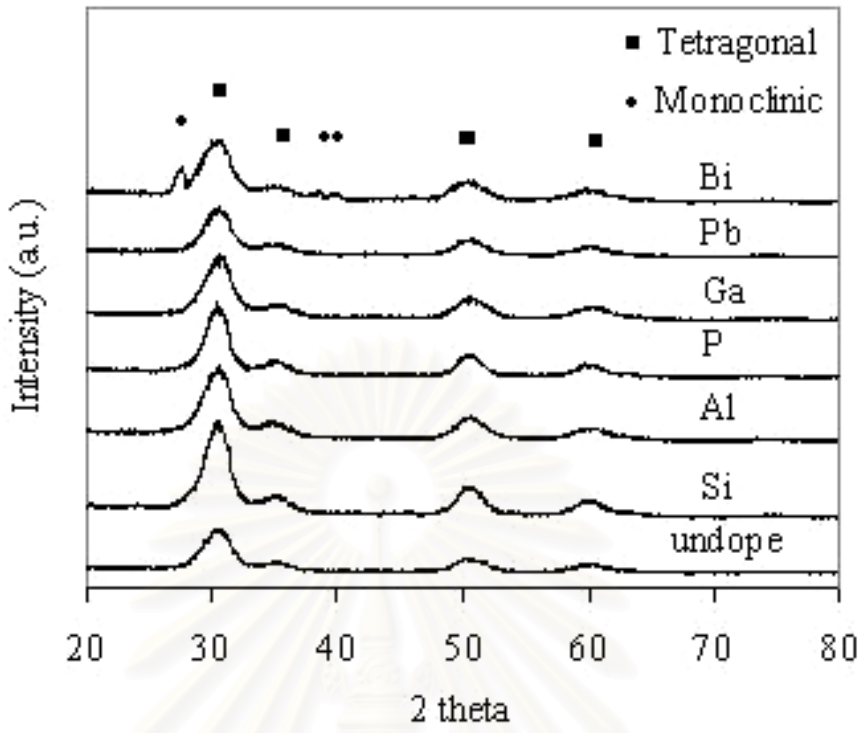

Figure 5.27 The XRD patterns for the second element doped zirconia at 0.02 ratio of metal/Zr.

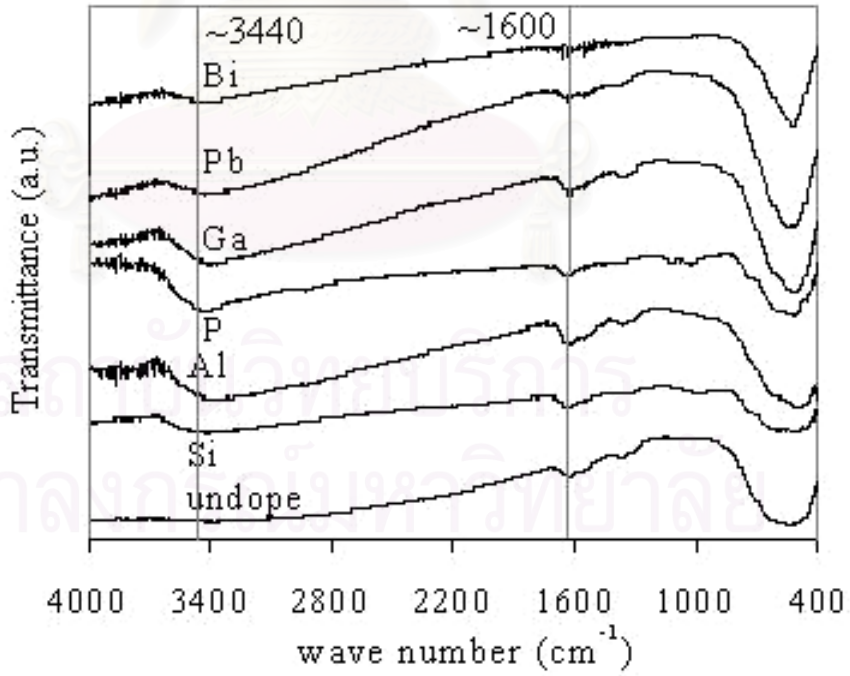

Figure 5.28 IR spectra of the second element doped zirconia at metal/Zr ratio of 0.02.

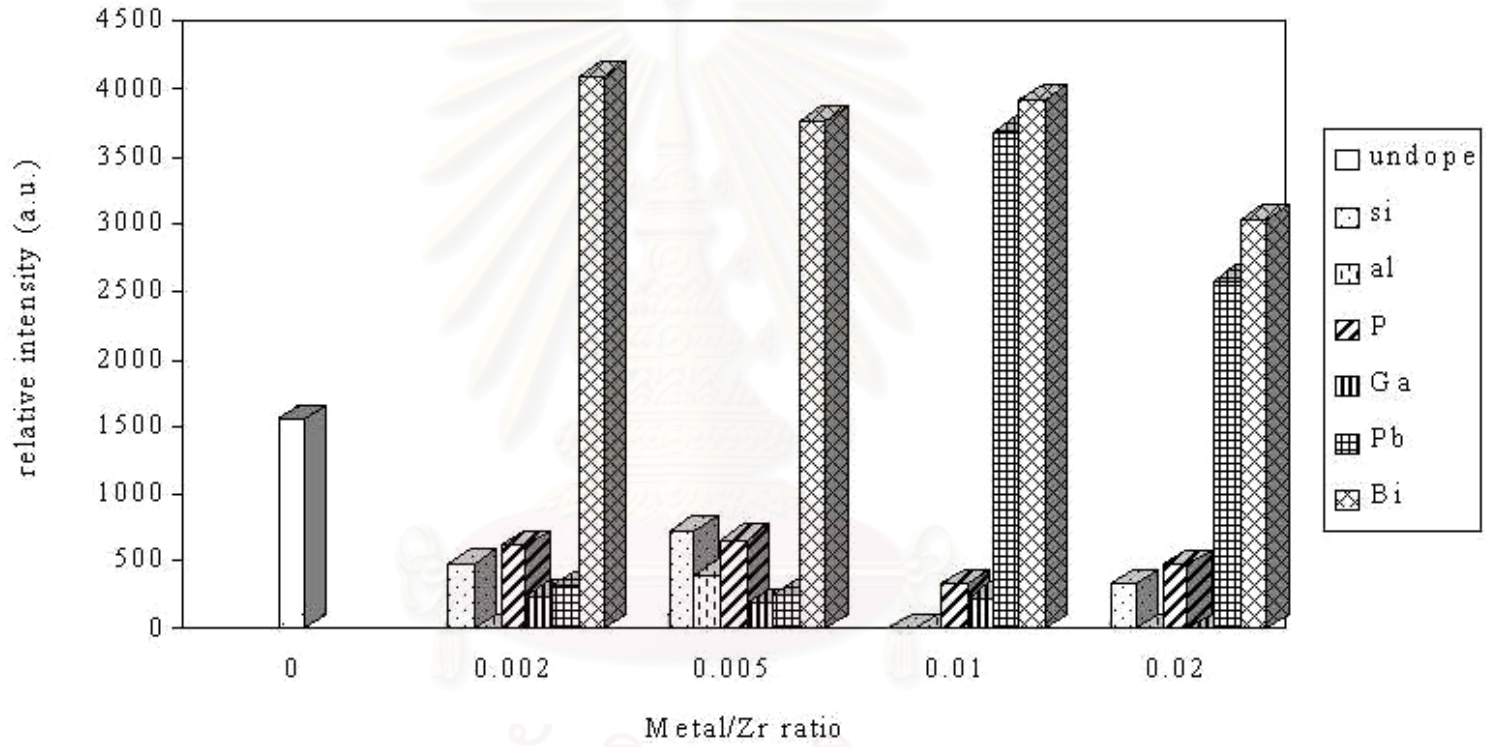

Figure 5.29 Bar diagram shows relative ESR intensity of second element doped zirconia at various ratios of metal/Zr

CHAPTER VI

CONCLUSIONS AND RECOMMENDATION

6.1 Conclusions

The conclusions of the present research are the following:

1. The ionic size of dopant had an effect on Zr^{3+} intensity assumed as defect of zirconia structure. In comparison with Zr ionic size, the smaller ionic size of dopant caused to decrease of Zr^{3+} intensity, on the other hand, increasing of the intensity arose from doping of the larger ionic dopant such as Bi and Pb.

2. The intensity of hydroxyl groups detected by IR spectroscopy represented opposite to Zr^{3+} intensity, however it correlated significantly to the amount of CO_2 desorption.

3. Adding dopant affected on surface area of zirconia. The smaller size doping maintained surface area in contrast, the larger size doping resulted in extremely decreasing of surface area.

4. Doping with bismuth made zirconia structure to be more thermodynamically stable.

Table 6.1 Conclusion on the effect of the second element added zirconia

The second element	Effect of adding the second element
Oversize than Zr	Higher amount of Zr^{3+} Decreasing of surface area dramatically
Lowersize than Zr	Increasing of hydroxyl group
Range of ionic size; P < Si < Al < Ga < Zr < Pb < Bi	

6.2 Recommendation for future study

From the previous conclusions, the following recommendations for the future study are proposed.

1. To study phase and thermal stability of the various type of the second element modified zirconia.

2. To study hydrophilic properties of ZrO_2 surface with dopants.

REFERENCES

ศิรรัตน์ คงวุฒิติ. กลไกการตกผลึกของเซอร์โคเนียภายใต้ภาวะไกลโคเทอร์มอลและผลของซิลิกาต่อความเสถียรทางความร้อนและพื้นที่ผิวของเซอร์โคเนียที่ดัดแปร. วิทยานิพนธ์ปริญญาดุษฎีบัณฑิต, ภาควิชาวิศวกรรมเคมี บัณฑิตวิทยาลัย จุฬาลงกรณ์มหาวิทยาลัย. 2002.

Adamski, A.; Sojka, Z.; Dyrek, Z.; Che, M. An XRD and ESR study of V_2O_5/ZrO_2 catalysts: influence of the phase transitions of ZrO_2 on the migration of V^{4+} ions into zirconia. Solid State Ionics 177 (1999): 113-122.

Aylward, G. and Findlay, T. SI Chemical data, fifth edition (Singapore: CMO Image Printing Enterprise, 2002), pp. 6-13.

Bikramjit, B.; Jozef, V.; Omer, V. D. B. Transformation behavior of tetragonal zirconia: role of dopant content and distribution. Materials Science and Engineering A366 (2004): 338-347.

Bokhimi, X.; Morales, A.; Novaro, O.; Portilla, M.; Lopez, T.; Tzompantzi, F.; Gomez, R. Tetragonal nanophase stabilization in nondoped sol-gel zirconia prepared with different hydrolysis catalysts. Journal of Solid State Chemistry 135 (1998): 28-35.

Boulouz, M.; Martin, L.; Boulouz, A.; Boyer, A. Effect of the dopant content on the physical properties of Y_2O_3-ZrO_2 and CaO-ZrO_2 thin films produced by evaporation and sputtering techniques. Materials Science and Engineering B67 (1999): 122-131.

Caili, S.; Junrong, L.; Dehua, H.; Zhengxing, C.; Qiming, Z. Synthesis of isobutene from synthesis gas over nanosize zirconia catalysts. Applied Catalysis A: General 202 (2000): 81-89.

Capel, F.; Moure, C.; Duran, P.; Gonzalez, E. A. R.; Caballero, A. Structure-electrical properties relationships in TiO_2-doped stabilized tetragonal zirconia ceramics. Ceramics International 25 (1999): 639-648.

Carlos, R. V.; Carlos, L. P.; Kiyoyuki, S.; Carlos, A.; Jose, M. P. Coking of SO_4^{2-}-ZrO_2 Catalysts during isomerization of n-butane and its relation to the reaction mechanism. Journal of Catalysis 187 (1999): 39-49.

Carlos, R. V.; Carlos, L. P.; Kiyoyuki, S.; Jose, M. P. Tetragonal structure, anionic vacancies and catalytic activity of SO_4^{2-} -ZrO_2 catalysts for n-butane isomerization. Applied Catalysis A: General 230 (2002): 137-151.

Cerrato, G.; Bordiga, S.; Barbera, S.; Morterra, C. Surface characterization of monoclinic ZrO_2 I. Morphology, FTIR spectral features, and computer modelling. Applied Surface Science 115 (1997): 53-65.

Chen, F. R.; Coudurier, G.; Joly, J. R., Vedrine, J. C. Superacid and catalytic properties of sulfated zirconia. Journal of catalysis 143 (1993): 616-626.

Das, D.; Mishra, H. K.; Parida, K. M.; Dalai, A. K. Preparation, physico-chemical characterization and catalytic activity of sulphated ZrO_2-TiO_2 mixed oxides. Journal of Molecular Catalysis A: Chemical 189 (2002): 271-282.

Davydov Anatoli, Molecular Spectroscopy of Oxide Catalyst Surfaces (England: John Wiley & Sons Ltd., 2003), pp. 77-94.

Diez, V. K.; Apesteguia, C. R.; Dicosimo, J. I. Effect of the chemical on catalytic performance of Mg_yAlO_x catalysts for alcohol elimination reactions. Journal of Catalysis 215 (2003): 220-233.

Dongare, M. K.; Ramaswamy, V.; Gopinath, C. S.; Ramaswamy, A. V.; Scheurell, S.; Brueckner, M.; Kemnitz, E. Oxidation activity and ^{18}O-Isotope exchange behavior of Cu-stabilized cubic zirconia. Journal of Catalysis 199 (2001): 209-216.

Dove Martin, Structure and Dynamics: an atomic view of materials (Great Britain: Oxford university Press, 2003), pp. 274-276.

Eguchi, K.; Akasaka, N.; Mitsuyasu, H.; Nanaka, Y. Process of solid state reaction between doped ceria and zirconia. Solid State Ionics 135 (2000): 589-594.

Elisabeth, D.; Florence, B.; Guihem, D.; Pierre B. Quantification of chemical pressure in doped nanostructured zirconia ceramics. Journal of Physical Chemistry B 107 (2003): 8321-8326.

Francisco, D. M.; Willa, L.; John, D. M. Chemical interactions promoting the ZrO_2 tetragonal stabilization in ZrO_2-SiO_2 Binary Oxides. Journal of the American Ceramic Society 83 (2000): 1506-1512.

Friederike, C. J.; Alexander, H.; Jutta, K.; Gisela, L.; Rolf, E. J.; Thorsten, R.; Ute, W.; Robert, S.; Carmen, H.; Klaus, K. Incorporation of manganese and iron into the zirconia lattice in promoted sulfated zirconia catalysts. Journal of Catalysis 224 (2004): 124-137.

Garvie, R. C. The occurrence of metastable tetragonal zirconia as a crystallite size effect. The Journal of Physical Chemistry 82 (1978): 218-224.

Garvie, R. C. Stabilization of the tetragonal structure in zirconia microcrystals. The Journal of Physical Chemistry 69 (1965): 1238-1243.

Hartridge, A.; Ghanashyam, M.; Bhattacharya, A. K. Temperature and ionic size dependence on the structure and optical properties of nanocrytalline lanthanide doped zirconia thin films. Thin Solid Films 384 (2001): 254-260.

Hunter, B. A.; Howard, C. J.; Kim, D. J. Bond valence analysis of tetragonal zirconias. Journal of Solid State Chemistry 146 (1999): 363-368.

Iglesia, E.; Barton, D. G.; Biscardi, J. A.; Gines, M. J. L.; Soled, S. L. Bifunctional pathways in catalysis by solid acids and bases. Catalysis Today 38 (1997): 339-360.

Jagadish, C. R.; Chitta, R.; Panchanan, P. Chemical synthesis of nanocrystalline tin-doped cubic ZrO_2 powders. Material Letters 57 (2003): 2140-2144.

Jang, J. W.; Kim, H. K.; Lee, D. Y. The effect of tetravalent dopants on the unit cell volume of 2Y-TZP and 8Y-SZ. Material Letters 58 (2004): 1160-1163.

Ken-ichi, M.; Teruaki, K.; Tomoki, H.; Lianhai, L.; Masatomo, Y. Active sites on ZrO_2 for the formation of isobutene from CO and H_2. Journal of Molecular Catalysis A: Chemical 159 (2000): 97-102.

Khor, K. A.; Yang, J. Lattice parameters, tetragonal (c/a) and transformability of tetragonal zirconia phase in plasma-sprayed ZrO_2-Er_2O_3 coatings. Material Letters 31 (1997): 23-27.

Kongwudthiti, S.; Praserthdam, P.; Silveston, P.; Inoue, M. Influence of synthesis conditions on the preparation of zirconia powder by the glycothemal method. Ceramics International 29 (2003): 807-814.

Kongwudthiti, S.; Tanakulrungsank, W.; Inoue, M.; Praserthdam, P. Synthesis of large surface area silica-modified zirconia by the glycothermal method. Journal of Materials Science Letters 21 (2002): 1461-1464.

Kongwudthiti, S.; Tanakulrungsank, W.; Inoue, M.; Praserthdam, P. The influence of Si-O-Zr bonds on the crystal-growth inhibition of zirconia prepared by the glycothermal method. Journal of Materials Processing Technology 136 (2003): 186-189.

Lee, J. H.; Yoon, S.M.; Kim, B. K.; Kim, J.; Lee, H. W.; Song, H. S. Electrical conductivity and defect structure of yttria-doped ceria-stabilized zirconia. Solid State Ionics 144 (2001): 175-184.

Liu, H.; Feng, L.; Zhang, X.; Xue, Q. ESR Characterization of ZrO_2 nanopowder. The Journal of Physical Chemistry 99 (1995): 332-334.

Loong, C. K. and Ozawa, M. The role of rare earth dopants in nanophase zirconia catalyst for automotive emission control. Journal of Alloys and Compounds 303-304 (2000): 60-65.

Manriquez, M. E.; Lopez, T.; Gomez, R.; Navarrete, J. Preparation of TiO_2-ZrO_2 mixed oxides with controlled acid-basic properties. Journal of Molecular Catalysis A: Chamical 220 (2004) 229-237.

Moran, P. M.; Castillo, S.; Lopez, T.; Gomez, R.; Cordero, B.; Novaro, O. Synthesis, characterization and catalytic activity in the reduction of NO by CO on alumina-zirconia sol-gel derived mixed oxides. Applied Catalysis B. Environmental 21 (1999): 79-88.

Morterra, C.; Giamello, E.; Orio, L.; Volante, M. Formation and reactivity of Zr^{3+} centers at the surface of vacuum-activated monoclinic zirconia. The Journal of Physical Chemistry 94 (1990) 3111-3116.

Punnoose, A.; Seehra, M. S. ESR observation of W^{5+} and Zr^{3+} states in $Pt/WO_x/ZrO_2$ catalysts. Catalysis Letters 78 (2002) 157-160.

Qin, Z.; Xinping, W.; Tianxi, C. The study of surface properties of ZrO_2. Applied Surface Science 225 (2004): 7-13.

Rose, M.; Balogh, A.G.; Hahn, H. Instability of irradiation induced defects in nanostructured materials. Nuclear Instruments and Methods in Physics Research B 127/128 (1997): 119-122.

Silvia, G. B.; Jose, A. N.; Maria, C. H.; Gloria, M. R.; Marta, I. L. Photocatalytic properties of ZrO_2 and Fe/ZrO_2 semiconductors prepared by a sol-gel technique. Journal of Photochemistry and Photobiology A: Chemistry 129 (1999): 89-99.

Sohn, J. R.; Cho, S. G.; Pae, Y.; Hayashi, S. Characterization of vanadium oxide-zirconia catalyst. Journal of Catalysis 159 (1996): 170-177.

Takeuchi, K.; Perry, S. S.; Salmeron, M.; Somorjai, G. A. The bonding properties of hydrogenated and fluorinated molecules to zirconium oxide thin films: influence of surface defects and water coadsorption. Surface Science 323 (1995): 30-38.

Torralvo, M. J. and Alario, M. A. Crystallization behavior of zirconium oxide gels. Journal of Catalysis 86 (1984): 473-476.

Valmalette, J. CH. and Isa, M. Size effects on the stabilization of ultrafine zirconia nanoparticles. Chemistry Materials 14 (2002): 5098-5102.

Vladimir, V. S. and Markus, W. Aluminium-doped zirconia nanopowders: Chemical vapor synthesis and structural analysis by Rietveld refinment of X-ray diffraction data. Chemistry Materials 15 (2003): 2668-2674.

Wang, J. A.; Valenzuela, M. A.; Bokhimi, X. Crystalline structure refinements of a series of catalytic materials with the Rietveld technique. Colloids and Surfaces A: Physicochemical and Engineering Aspects 179 (2001): 221-227.

Wei, P. D.; Yu, P. W.; Ta, J. H. Yttria-stabilized zirconia supported copper oxide catalyst. Journal of Catalysis 160 (1996): 155-170.

Wen, K. C.; Andy, A. W.; Yuan, H. L. Oxygen-induced structure change of zirconia by adding rare earth oxides with solid state method. Journal of Alloys and Compounds 249 (1997): 251-255.

West Anthony, Solid State Chemistry and it's Applications (Singapore: John Wiley & Sons Ltd., 1989).

Yinghong, Y.; Xiping, Z.; Weiming, H.; Zi, G. Nanosized titania and zirconia as catalysts for hydrolysis of carbon disulfide. Applied Catalysis B: Environmental (2003).

Yingwei, L.; Dehua, H.; Qijian, Z.; Boqing, X.; Qiming, Z. Erratum to "Influence of reactor materials on i-C_4 synthesis from CO hydrogenation over ZrO_2 based catalysts". Fuel Processing Technology 85 (2004): 401-411.

Yingwei, L.; Dehua, H.; Qijian, Z.; Xin, Z.; Boqing, X. Effects of redox properties and acid-base properties on isosynthesis over ZrO_2-based catalysts. Journal of Catalysis 221 (2004): 584-593

Yingwei, L.; Dehua, H.; Yubin, Yuan.; Zhenxing, Cheng.; Qiming, Zhu. Influence of acidic and basic properties of ZrO_2 bases catalysts on isosynthesis. Fuel 81 (2002): 1611-1617.

Yongde, X.; Weiming, H.; Zi, G. A new catalyst for n-butane isomerization: Persulfate-modified Al_2O_3-ZrO_2. Applied Catalysis A: General 185 (1999): 293-300.

Yoshida, H.;Chaskar, M. G.; Kato, Y.; Hattori, T. Active sites on silica-supported zirconium oxide for photoinduced direct methane conversion and photoluminescence. Journal of Photochemistry and Photobiology A: Chemistry 160 (2003): 47-53.

Zhao, Q.; Shih, W. H.; Chang, H. L.; Andersen, P. The effect of curing on the thermal stability of Si-doped ZrO_2 powders. Applied Catalysis A: General 262 (2004): 215-221.

Zhao, Q.; Wang, X.; Cai, T. The study surface properties of ZrO_2. Applied Surface Science 225 (2004): 7-13.

Zhou, Z.; Zhang, Y.; Tierney, J. W.; Wender, I. Hybrid zirconia catalysts for conversion of Fischer-Tropsch waxy products to transportation fuels. Fuel Processing Technology 83 (2003): 67-80.

APPENDICES

APPENDIX A

CALCULATION OF THE AMOUNT OF THE REAGENT REQUIRED FOR THE REACTION

In this study, the second element added in zirconia with various molar ratios were prepared using 1,4-butanediol as the solvent, and therefore detailed calculation procedure of silicon doped zirconia is given here.

Calculation of the amount of TEOS for silicon doped zirconia preparation

Zirconium tetra *n*-propoxide (ZNP) and tetraethyl orthosilicate (TEOS) are used as the reactants to prepare silicon doped zirconia.

1. Zirconium *n*-propoxide [$Zr(OC_3H_7)_4$] has a molecular weight of 327.57 g/mol.
   Zirconium, Zr, has an atomic weight of 91.22 g/mol.
2. Tetraethyl orthosilicate [$(C_2H_5O)_4Si$] has a molecular weight of 208.33 g/mol
   Silicon, Si, has an atomic weight of 28.0855 g/mol.

Example: Calculation of preparation of silicon doped zirconia with the molar ratio Si/Zr of 0.02 are as follows:

Seven gram of zirconium *n*-propoxide was used for the preparation of silicon doped zirconia with a molar ratio Si/Zr of 0.02.

Zirconium *n*-propoxide 7 g was consisted of zirconium equal to:

Zirconium = 7/327.57 = 0.0214 mol

To get the product with molar ratio Si/Zr of 0.02;

Silicon = 0.02 x 0.0214 mol = 0.00043 mol

Tetraethyl orthosilicate reqired is equal to: 208.33 x 0.00043 = 0.0890 g

APPENDIX B

CALCULATION OF THE CRYSTALLITE SIZE

Calculation of the crystallite size by Debye-Scherrer equation

The crystallite size was calculated from the half-height width of the diffraction peak of XRD pattern using the Debye-Scherrer equation.

From Scherrer equation:

$$D = \frac{K\lambda}{\beta \cos \theta} \qquad \text{(B.1)}$$

where D = Crystallite size, Å

K = Crystallite-shape factor = 0.9

λ = X-ray wavelength, 1.5418 Å for CuKα

θ = Observed peak angle, degree

β = X-ray diffraction broadening, radian

The X-ray diffraction broadening (β) is the pure width of a powder diffraction free from all broadening due to the experimental equipment. α-Alumina is used as a standard sample to observe the instrumental broadening since its crystallite size is larger than 2000 Å. The X-ray diffraction broadening (β) can be obtained by using Warren's formula.

From Warren's formula:

$$\beta = \sqrt{B_M^2 - B_S^2} \qquad \text{(B.2)}$$

Where B_M = The measured peak width in radians at half peak height.

B_S = The corresponding width of the standard material.

Example: Calculation of the crystallite size of zirconia

The half-height width of 111 diffraction peak = 1.83^o (from the figure B.1)

= $(2\pi x180)/360$

= 0.0319 radian

The corresponding half-height width of peak of α-alumina (from the Bs value at the 2θ of 30.3^o in figure B.2) = 0.0043 radian

The pure width, $\beta = \sqrt{B_M^2 - B_S^2}$

$= \sqrt{0.0319^2 - 0.0043^2}$

= 0.0316 radian

B = 0.0316 radian

2θ = 30.3^o

θ = 15.15^o

λ = 1.5418 Å

The crystallite size = $\frac{0.9x\,1.5418}{0.0316\,\cos 15.15}$ = 45.49 Å

= 4.5 nm

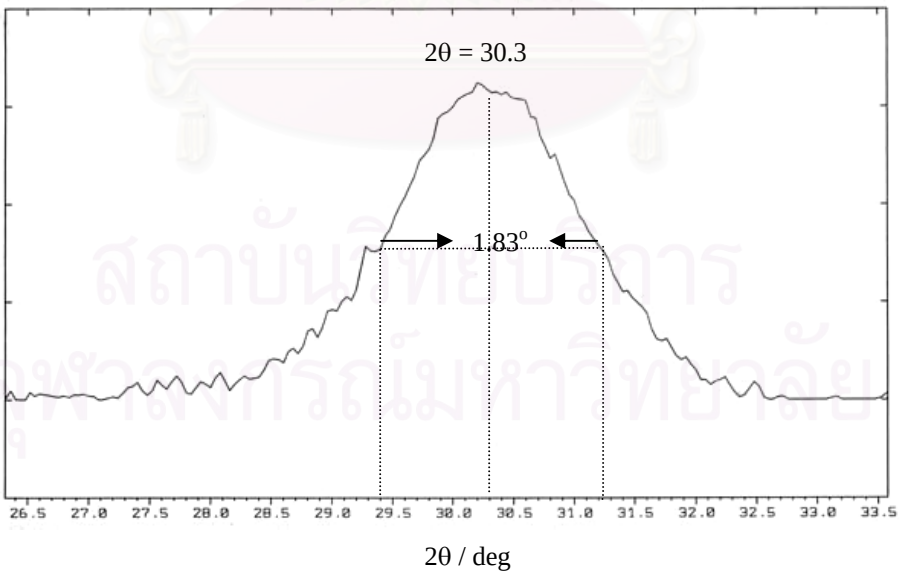

Figure B.1 The 111 diffraction peak of zirconia for calculation of the crystallite size

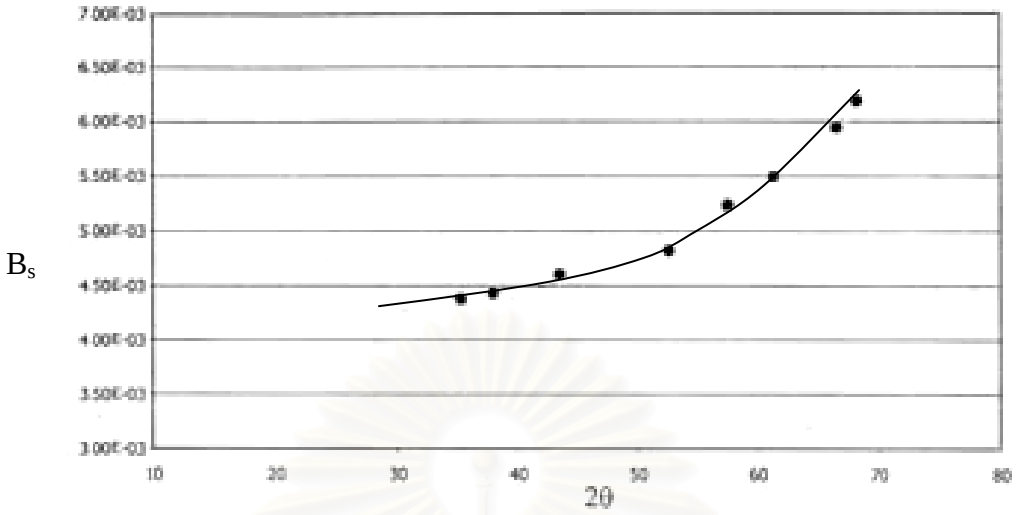

Figure B.2 The plot indicating the value of line broadening due to the equipment. The data were obtained by using α-alumina as a standard

APPENDIX C

CALCULATION OF BET SURFACE AREA BY THE SINGLE POINT METHOD

From Brunauer-Emmett-Teller (BET) equation:

$$\frac{X}{V(1-X)} = \frac{1}{VmC} + \frac{(C-1)X}{VmC} \qquad (C.1)$$

Where: X = relative partial pressure of N_2, P/P_o

P_o = saturated vapor pressure of N_2 (or adsorbed gas) at the experimental temperature

P = equilibrium vapor pressure of N_2

V = volume of gas adsorbed at a pressure P; ml at the NTP/ g of sample

V_m = volume of gas adsorbed at monolayer, ml. at the NTP / g of sample

C = constant

Assume $C \rightarrow \infty$, then

$$\frac{X}{V(1-X)} = \frac{X}{Vm} \qquad (C.2)$$

$$Vm = V(1-P/P_o)$$

From the gas law,

$$\frac{P_bV}{273} = \frac{P_tV}{T} \qquad (C.3)$$

Where: V = constant volume

P_b = pressure at 0 ^oC

P_t = pressure at t ^oC

T = 273.15 + t, K

P_t = 1 atm and thus, P_b = (273.15 / T)

Partial pressure of Nitrogen:

$$P = \frac{[\text{Flow of } (He+N_2) - \text{Flow of } He]}{\text{Flow of } (He+N_2)} \times \quad (C.4)$$

$$= 0.3 \text{ atm}$$

N_2 saturated vapor pressure, P_o = 1.1 atm

$$p = P / P_o = P / 1.1 = 0.3/1.1 = 0.2727$$

How to measure V

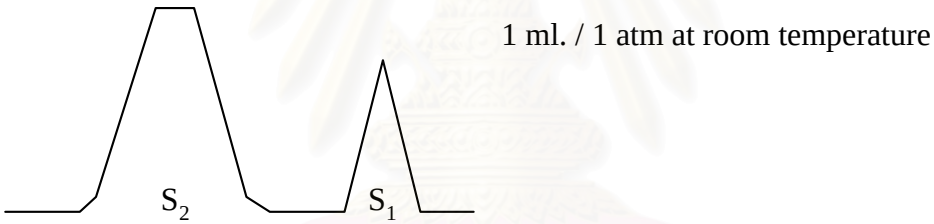

$$V = \frac{S_2}{S_1} \times \frac{1}{W} \times \frac{273.15}{T} \text{ ml. / g of catalyst} \quad (C.5)$$

Where, S_1 = Nitrogen 1 ml/1 atm of room temperature area

S_2 = Desorption of nitrogen area

W = Weight of the sample (g)

T = Room temperature (K)

Therefore,

$$Vm = \frac{S_2}{S_1} \times \frac{1}{W} \times \frac{273.15}{T} \times (1-p)$$

$$Vm = \frac{S_2}{S_1} \times \frac{1}{W} \times \frac{273.15}{T} \times 0.7273 \qquad \text{(C.6)}$$

Surface area of catalyst:

$$S = \frac{N\sigma V_m}{M}$$

Where, N = Avogadro's number = 6.02×10^{23}

σ = area occupied by one molecule of adsorbed nitrogen = 16.2×10^{-20}

M = volume of one mole nitrogen = 22410 cm^3/mol

Then,

$$S = 4.352\ Vm$$

$$S = \frac{S_2}{S_1} \times \frac{1}{W} \times \frac{273.15}{T} \times 0.7273 \times 4.352$$

$$S = \frac{S_2}{S_1} \times \frac{1}{W} \times \frac{273.15}{T} \times 3.1582 \qquad \text{(C.7)}$$

APPENDIX D

LIST OF PUBLICATION

Jantana Wiwattanapongpan, Okorn Mekasuwandumrong and Piyasan Praserthdam, “Effects of types and amount of the second element added in glycothermally synthesized zirconium dioxide”, Regional Symposium on Chemical Engineering 2004, Bangkok, Thailand, December 1-3, 2004, NS-231.

EFFECTS OF TYPES AND AMOUNT OF THE SECOND ELEMENT ADDED IN GLYCOTHERMALLY SYNTHESIZED ZIRCONIUM DIOXIDE ON ADSORPTION OF CARBON DIOXIDE

Jantana Wiwattanapongpan[a], Okorn Mekasuwandumrong[b] and Piyasan Praserthdam[a,*]

[a]Center of Excellence on Catalysis and Catalytic Reaction Engineering,
Department of Chemical Engineering, Faculty of Engineering,
Chulalongkorn University, Bangkok 10330, THAILAND
[b]Department of Chemical Engineering
Faculty of Engineering and Industrial Technology,
Silpakorn University, Nakhonpathom, Thailand
*Corresponding author: E-mail address: piyasan.p@chula.ac.th

Abstract

Zirconium dioxide (ZrO_2) or zirconia was synthesized by glycothermal method which adding a small amounts of the second elements (such as Si, Al, P, Ga, Pb, Bi) in crystal structure. The crystal structure and crystallite size were determined by XRD. Morphologies of all products were observed by SEM. The basic sites of zirconia were studied by CO_2-TPD. The results suggested that doping elements affect certainly lattice deformation and the basic property of zirconia. In addition, the doped zirconia in appropriate quantity exhibited higher basic sites. The amount of adsorbed CO_2 on zirconia surface at various metal/zirconia ratios related to the amount of lattice defects in zirconia. When the ionic radius of the second element larger than Zr^{4+}, zirconia rarely adsorb CO_2.

Keywords: Zirconium dioxide, dopants

1. Introduction

Zirconia is an important material and has obtained much interest in industry [1]. It have three polymorphs; monoclinic, tetragonal and cubic. Two later are metastable and exist at room temperature due to the presence of chemical impurities (type and amount), the preparation conditions [2] and grain size concerning surface energy [3]. The surface energy of finite size particles is strongly influenced by the presence of surface defects, adsorbed species and the edge effect resulting from a faceted morphology [4]. Nanosize crystals were interesting because of their large surface areas, surface defects, etc [5]. It has high thermal and chemical stability, high strength and toughness [3], corrosion resistance as well as low conductivity. It is employed for ceramics, electronics including catalysis such as catalysts and catalyst supports [1,6], since it has weak acidic and basic properties The basic sites would be necessary catalytic sites to remove active hydrocarbon from the intermediates in the isosynthesis [5].

The study of defect by adsorbing probe molecules has contributed to the understanding of the active sites [7]. Defects were found to change the characteristics of the adsorption of some molecule [7]. The influence of defects are expected to effect the adsorption of the oxide surface [8]. In the previous work, Fe-containing ZrO_2 prepared by a sol-gel technique shown the presence of ion could modify the surface properties of the material regarding the type of active sites, presence of defect, which could increase the adsorption [9]. Doping effects on the nature of aggregation of nanoparticles, defect formation, crystal phase transformation in ZrO_2 [10].

In this paper, we pay attention on adding the small amount of various dopants effect the adsorption of carbon dioxide on the surface of zirconia that involving to the defect formation of zirconia from adding dopants in lattice.

2. Experimental

Powder preparation

Mixtures of Zirconium tetra-*n*-propoxide and dopant precursors (tetra-ethyl-otho-silicate, Aluminium isopropoxide, tetraethyphosphate, Gallium (III) acetylacetonate, Lead (IV) acetate and Bismuth (III) acetate) were suspended in 100 mL of 1,4 butanediol in a test tube, which was then placed in a 300 mL autoclave. The gap between the test tube and the autoclave wall was filled with 30 mL of 1,4 butanediol. The autoclave was purged completely by nitrogen before heating up to 300°C at a rate of 2.5°C/min. Autogeneous pressure during the reaction gradually increased as the temperature was raised. The temperature was held constant for 2 h. After the reaction, autoclave was cooled down to room temperature, the resulting powders were repeatedly washed with methanol and dried in air. The molar ratios of dopants were varied from 0 to 0.02.

Characterization

The powders were characterized by X-ray diffraction spectroscopy (XRD) to identify crystal structure. The crystallite size was calculated by using the Scherrer equation. The morphology of secondary particle was observed by Scanning electron microscopy (SEM). The basicity of samples was measured by CO_2-TPD technique. Sample was heated in He flow at 400 ^oC for 1 h to remove the surface impurities. The sample was saturated in CO_2 (30 ml/min) at 100 ^oC for 1 h. After saturation, the temperature was increased from 100-400 ^oC at a rate of 10 ^oC/min. The amount of desorbed CO_2 was determined by measuring the areas of the desorption profiles.

3. Results and discussion

3.1. Characterization by XRD

To examine the effect of adding dopants, the mole ratios of metal/Zr were varied from 0 - 0.02. Figs. 1 shows the XRD patterns for metal doped zirconia powders prepared via glycothermal method with vary molar ratio of metal/Zr. All spectra exhibited the typical pattern for tetragonal phase unless Bi-doped zirconia containing a tetragonal phase and a minor monoclinic phase due to lower valency and bigger size of this ion in comparison with Zr^{4+} (Bi^{3+} 1.11 Å and Zr^{4+} 0.84 Å for eight coordination number were shown in Table 1) lead instability in the lattice at lower temperatures and help to reorganise ZrO_2 to more thermodynamically stable polymorphs introducing some monoclinic phase in the powder [11]. Crystallite size of all zirconia samples were nearly size about 3 nm. The lattice parameters of doped ZrO_2 changed from undoped ZrO_2.

Table 1 Shown the ionic radius and ion charge of the elements [12].

Element	Ion charge	Ionic radius (Å)		
		Coordination number		
		4	6	8
Zr	4+	0.59	0.72	0.84
Si	4+	0.26	0.4	
Al	3+	0.39	0.535	
P	3+		0.44	
	5+	0.17	0.38	
Ga	2+		1.2	
	3+	0.47	0.62	
Pb	2+	0.98	1.19	1.29
	4+		0.78	0.94
Bi	3+		1.03	1.11
	5+		0.76	

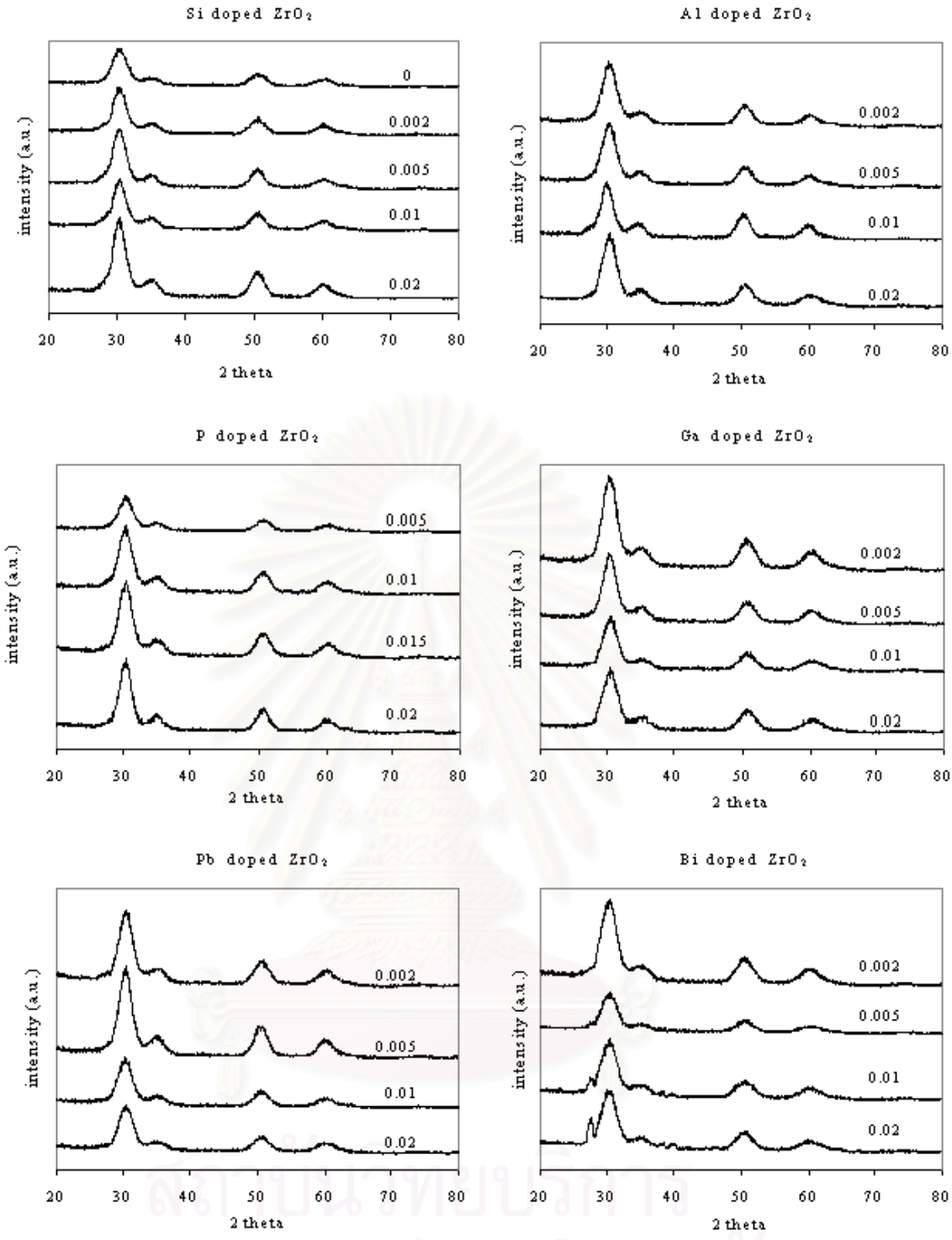

Fig. 1 The XRD patterns for metal-doped zirconia with vary molar ratio of metal/Zr.

3.2. Characterization by SEM

SEM micrographs of ZrO_2 and metal-doped ZrO_2 were shown in Fig. 2. Morphologies of ZrO_2 were spherical particle formed by aggregations of primary particles. In the part of metal doped ZrO_2 at molar ratio of 0.02, doping Si, Al, Ga and Bi had no effects on morphology of ZrO_2, spherical shape were still observed. Whiles aggregation of microspheres and agglomeration of small aggregates were observed in SEM image for P-doped ZrO_2. Unusual SEM micrographs of doping Pb at 0.005 and 0.02 mole ratio in Fig. 4 shown difference between agglomeration size of Pb doped ZrO_2 at 0.005 occurred more than at 0.02 mole ratio.

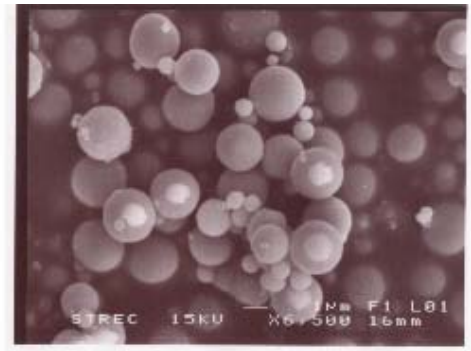

undoped ZrO_2

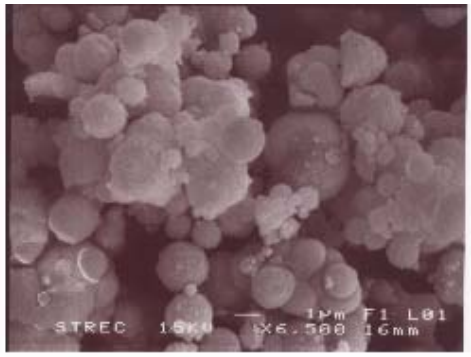

Si-doped ZrO_2

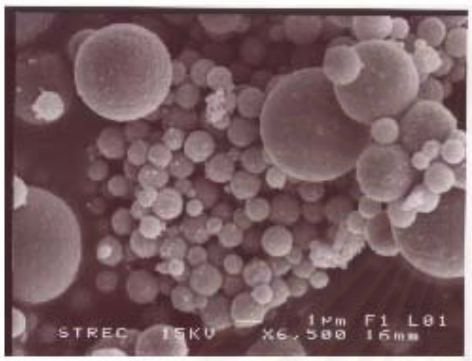

Al-doped ZrO_2

P-doped ZrO_2

Ga-doped ZrO_2

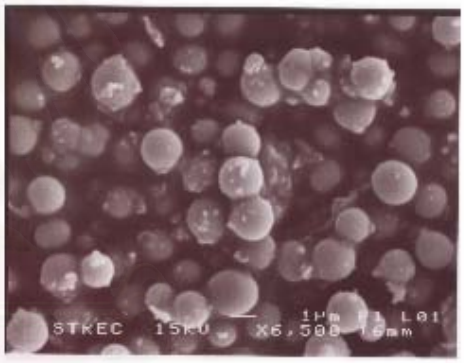

Bi-doped ZrO_2

Pb-doped ZrO_2 (0.005)

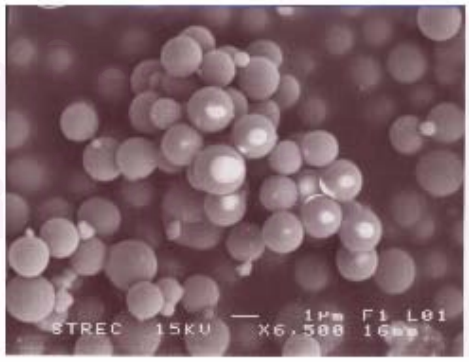

Pb-doped ZrO_2 (0.02)

Fig. 2 SEM micrographs of metal doped ZrO_2 for 0.02 mole ratio.

3.3. Characterization by CO_2-TPD

The amounts of desorbed CO_2 are summarized in Table 2. It was found that amount of desorbed CO_2 depend on doping ratio of dopants. At low metal/Zr ratio appeared better adsorption than at large ratio that may be optimization of doping. Moreover, ionic radius of each ions have many effects on adsorption CO_2-TPD. Bi-doped ZrO_2 have poor CO_2-adsorption and Pb-doped ZrO_2 at metal/Zr ratio 0.01 and 0.02 were not adsorption on zirconia surface. From the Table 1, Considering the same charge 4+ of Si and Pb, ionic radius of Si is smaller size than Pb and amount of desorbed CO_2 of Si-doped ZrO_2 higher than Pb which the results are the same with Al, Ga and Bi. The ionic radius of Pb and Bi are larger than another. It would concern on size effect of dopant's ion. The chemisorption of CO_2 on oxide surfaces occurs with the participation of surface hydroxyl groups and coordinatively unsaturated surface cations [13]. CO_2 is small adsorbed acid molecule for characterization surface of basic site. Amount of desorbed CO_2 may indicate the defect quantity. Wang et al. [14-16,18] reported that MgO catalyst prepared via sol-gel method had magnesium defect, catalytic active sites, which related to the basic sites and thus to the dehydrogenation activity of isopropanol. Moreover, they [18] found the relationship between defect structure and basic site of alumina obtained by sol-gel. Dongare et al. [14] had reported on enhancement in catalytic activity in total oxidation using perovskite (ABO_3) was correlated with the defect structure and oxygen vacancies created because substitution of A and/or B site cation and Jie et al. [15] suggested that if cation sublattice substituted with non-oxidizable dopants may influence the defect formation. Occupying a Zr^{4+} with lower-valent-cation creates oxygen vacancies in order to balance the charge compensation [16-17]. So, Zr^{4+} might be substituted with smaller size ion of dopants in the lattice to create defect.

Table 2 Shown crystallite size and amount of desorbed CO_2 at various ratio and dopant.

Dopants	M/Zr ratio	Crystallite size (nm)	Amount of CO_2 (micromole)
undope	0	3.6	27.6
Si	0.002	3.6	79.8
	0.005	3.4	103.4
	0.01	3.6	77.6
	0.02	3.7	42.3
Al	0.002	3.2	56.9
	0.005	3.3	47.2
	0.01	3.3	86.1
	0.02	3.2	63.9
P	0.005	3.5	21.8
	0.01	4.0	51.8
	0.015	3.6	48.6
	0.02	4.1	52.7
Ga	0.002	3.0	23.8
	0.005	3.5	68.9
	0.01	3.3	24.8
	0.02	3.1	26.4
Pb	0.002	3.4	28.0
	0.005	4.0	28.5
	0.01	3.1	0.0
	0.02	3.3	0.0
Bi	0.002	3.0	2.7
	0.005	3.4	16.4
	0.01	2.9	9.2
	0.02	3.1	22.6

4. Conclusions

From the result mentioned above, the metal doped ZrO_2 were successfully synthesized by glycothermal reaction. The morphologies of samples were micro spherical shape with agglomeration of primary particles. Si, Al, Ga and Bi doped ZrO_2 did not affect the morphology of ZrO_2. While the microspheres and agglomerations of small aggregates were observed for P-doped ZrO_2 and the size of agglomeration of Pb-doped ZrO_2 was depended on the amount of dopant loading. It was found that, doping in suitable amount effects on CO_2 adsorption and defect formation, oxygen vacancies and surface hydroxyl groups. Bigger size of ions effect on poor CO_2 adsorption on ZrO_2 surface. It can be explained by the placement of smaller size ions in lattice have enough distance to form bonds between metal-O, while bigger size interfere in lattice by unformed bond.

Acknowledgements

We would like to acknowledge financial supports from National Research Council of Thailand, Thailand Research Fund, Commissions on Higher Education, and Graduate School of Chulalongkorn University.

References

[1] Pengcheng Y., Xiaochai C., Youchang X., Tiandou H., Jing Z., and Tao L., 'Extended X-ray Absorption Fine Structure Studies on Mixed-Phase Zirconia', J. Phys. Chem. B, 107, pp 6511-6513, (2003).

[2] Adamaski A., Sojka Z., Dyrek K., and Che M., 'An XRD and ESR of V_2O_5/ZrO_2 catalysts: Influence of the phase transition of ZrO_2 on the migration of V^{4+} ions into zirconia', Solid State Ionics, 117, pp 113-122, (1999).

[3] Bikramjit B., Jozef V., and Omer V.D.B., 'Transformation behavior of tetragonal zirconia: Role of dopant content and distribution', Materials Science and Engineering, A366, pp 338-347, (2004).

[4] Valmalette J.CH., and Isa M., 'Size Effects on the Stabilization of Ultrafine Zirconia Nanoparticle', Chem. Mater, 14, pp 5098-5102, (2002).

[5] Caili S., Junrong L., Dehua H., Zhengxing C., and Qiming Z., 'Synthesis of Isobutane from Synthesis Gas Over Nanosize Zirconia Catalysts', Applied Catalysis A:General, 202, pp 81-89, (2000).

[6] Sirirat K., Piyasan P., Peter S., and Masashi I., 'Influence of Synthesis Conditions on the Preparation of Zirconia Powder by the Glycothermal Method', Ceramics International, 29, pp 807-814, (2003).

[7] Enrique F.A. and Robert J.M., 'Role of Defects in the Adsorption of Aliphatic Alcohols on the TiO_2(110) Surface', J. Phys. Chem. B,106, pp 10680-10692, (2002).

[8] Takeuchi K., Perry S.S., Salmeron M., and Somorjai G.A., 'The bonding properties of hydrogenated and fluorinated molecules to zirconium oxide thin films: influence of surface defects and water coadsorption', Surface Science, 323, pp 30-38, (1995).

[9] Silvia G.B., Jose A.N., Maria C.H., Gloria M.R., and Marta I.L., 'Photocatalytic Properties of ZrO_2 and Fe/ZrO_2 Semiconductors Prepared by a Sol-Gel Technique', Journal of Photochemistry and Photobiology A:Chemistry, 129, pp 89-99, (1999).

[10] Bikramjit B., Jozef V., and Omer V.D.B., 'Transformation behavior of tetragonal zirconia: Role of dopant content and distribution', Materials Science and Engineering, A366, pp 338-347, (2004).

[11] Jagadish C.R., Chitta R.S., and Panchanan P., 'Chemical synthesis of nanocrystalline tin-doped cubic ZrO_2 powders', Matterials Letters, 57, pp2140-2144, (2003).

[12] John, A.D., LANGE'S Handbook of Chemistry. R.R. Donnelley & Sons Company, United States of America, (1972).

[13] Anatoli D., Molecular Spectroscopy of Oxide Catalyst Surface. John Wiley & Sons Ltd, English, (2003).

[14] Dongare M.K., Ramaswamy V., Gopinath C.S., Ramaswamy A.V., Scheurell S., Brueckner M., and Kemnitz E., 'Oxidation Activity and 18O-Isotope Exchange Behavior of Cu-Stabilized Cubic Zirconia', Journal of Catalysis, 199, pp 209-216, (2001).

[15] Jie X., Janet H.T., Rudiger D., 'Influence of impurities on the oxygen activity-dependent variation of the oxygen content of a commercial, CaO-doped ZrO_2', Solid State Ionics, 166, pp 199-205, (2004).

[16] Ray J.C., Pramanik P., and Ram S., 'Formation of Cr^{3+} stabilized ZrO_2 nanocrystals in a single cubic metastable phase by a novel chemical route with a sucrose-polyvinyl alcohol polymer matrix', Materials Letters, 48, pp 281-291, (2001).

[17] Lee J.H., Yoon S.M., Kim B.K., Lee H.W., and Song H.S., 'Electrical conductivity and defect structure of yttria-doped ceria-stabilized zirconia', Solid State Ionics, 144, pp 175-184, (2001).

[18] Wang J.A., Valenzuela M.A., and Bokhimi X., 'Crystalline refinements of a series of catalytic materials with the Rietveld technique', Colloids and Surfaces A: Physicochemical and Engineering Aspect, 179, pp 211-227, (2001).

VITA

Miss Jantana Wiwattanapongpan was born on March 9, 1981 in Chachoengsao, Thailand. She received her Bachelor Degree of Chemical Engineering from Faculty of Engineering, Burapha University, Chonburi, Thailand in March 2003. She continued her Master study in the same major at Chulalongkorn University, Bangkok, Thailand in June 2003.